CMS Technical Summary Report #90-6

ANALYSIS OF NEW PHENOMENA IN SHEAR FLOW OF NON-NEWTONIAN FLUIDS

David S. Malkus,
John A. Nohel, and
Bradley J. Plohr

UNIVERSITY OF WISCONSIN

CENTER FOR THE MATHEMATICAL SCIENCES

Center for the Mathematical Sciences
University of Wisconsin—Madison
610 Walnut Street
Madison, Wisconsin 53705

August 1989

(Received August 10, 1989)

Sponsored by

U. S. Army Research Office
P. O. Box 12211
Research Triangle Park
North Carolina 27709

National Science Foundation
Washington, DC 20550

Air Force Office of
Scientific Research
Washington, DC 20332

Approved for public release
Distribution unlimited

UNIVERSITY OF WISCONSIN - MADISON
CENTER FOR THE MATHEMATICAL SCIENCES

ANALYSIS OF NEW PHENOMENA IN SHEAR FLOW OF NON-NEWTONIAN FLUIDS*

David S. Malkus[1,2]
John A. Nohel[1,3]
Bradley J. Plohr[1,4]

CMS Technical Summary Report #90-6

August 1989

Abstract

Phase-plane and small-parameter asymptotic techniques are used to analyze systems of ordinary differential equations that describe the transient behavior of non-Newtonian fluids in shear flow. These systems approximate the partial differential equations that derive from three-dimensional balance laws and from differential constitutive models for highly elastic liquids. Two models are considered: one with a single relaxation time and small Newtonian viscosity; the other with two relaxation times and no Newtonian viscosity. Both possess the key feature that the variation of steady shear stress with strain rate is not monotone.

The analysis shows that both models exhibit several distinctive phenomena: spurt, shape memory, hysteresis, latency, and normal stress oscillations. The predictions for the spurt phenomenon agree quantitatively with experimental results for polymer melts; the other new phenomena, which were discovered recently in numerical simulation, should also be observable in rheological experiments.

AMS (MOS) Subject Classifications: 34C35, 34D10, 34E05, 35L60, 35L65, 35L67, 65M99, 65N30, 73F15, 76A05, 76A10

Key Words: quadratic ODE, phase plane, global dynamics, asymptotics, non-Newtonian shear flow, spurt, shape memory, hysteresis, latency

[1]Center for the Mathematical Sciences University of Wisconsin-Madison, Madison, WI 53705.
[2]also Department of Engineering Mechanics.
[3]also Department of Mathematics.
[4]also Computer Sciences Department.

*Supported by the U. S. Army Research Office under Grant DAALO03-87-K-0036, the National Science Foundation under Grants DMS-8712058 and DMS-8620303, and the Air Force Office of Scientific Research under Grants AFOSR-87-0191 and AFOSR-85-0141.

1. Introduction

The purpose of this paper is to analyze novel phenomena in dynamic shearing flows of non-Newtonian fluids that are important in polymer processing [15]. One striking effect, called the "spurt" phenomenon, was observed by Vinogradov *et al.* [17] in experiments concerning quasi-static flow of monodispersive polyisoprenes through capillaries. They found that the volumetric flow rate increases dramatically at a critical stress that is independent of molecular weight. Until recently, spurt has been associated with failure of the polymer to adhere to the wall [5]. The focus of our current research is an alternative explanation of spurt and related phenomena.

The present paper analyzes systems of ordinary differential equations that approximate the dynamics of one-dimensional shear flow of highly elastic non-Newtonian fluids at low Reynolds number. The analysis reveals several distinctive phenomena related to spurt: shape memory, hysteresis, latency, and normal stress oscillations. Furthermore, the comparison two different viscoelastic fluid models shows that the effect of a second relaxation time is similar to that of Newtonian viscosity.

The essential aspects of spurt experiments are reflected in one-dimensional shear flow through a slit die, which is governed by fluid balance laws and constitutive relations. The key feature of constitutive relations that exhibit spurt is a non-monotonic relation between the steady shear stress and strain rate. This causes jumps in the steady strain rate to form when the driving pressure gradient exceeds a critical value; such jumps correspond to the sudden increase in volumetric flow rate observed in the experiments of Vinogradov *et al.* The constitutive models we study derive from three-dimensional differential constitutive relations with multiple relaxation times (based on work of Johnson and Segalman [8] and of Oldroyd [14]). These models lead to systems of partial differential equations that are evolutionary, are globally well-posed (in a sense described below), and possess discontinuous steady states that explain spurt effects.

The Johnson-Segalman–Oldroyd shear flow equations were investigated using numerical simulation in Refs. [9, 11]. Transient flows at high Deborah (Weissenberg) number and low Reynolds number exhibited spurt, shape memory, and hysteresis. Moreover, other effects were evident, such as latency, normal stress oscillations, and molecular weight dependence of hysteresis. A principal conclusion is that satisfactory explanation of the spurt phenomenon requires understanding the full dynamics of the flow, not only steady flows. Furthermore it was shown [11] that the equations reduce to planar systems of ordinary differential equations in the flow regime appropriate to the spurt experiments. The objective of the present paper is to study the reduced dynamical systems using analytical methods and to verify the dramatic implications of numerical simulation.

Earlier work has drawn connections between spurt phenomena and non-monotone constitutive relations. Hunter and Slemrod [7] studied the qualitative behavior of discontinuous steady states in a simple one-dimensional viscoelastic model that exhibits spurt, shape memory, and hysteresis. Their model contrasts with the ones studied here, however, in that the effects observed in their model are related to the linear instability and loss of evolutionarity of the flow at certain Deborah numbers.

The two systems of partial differential equations that we use to model shear flow through slit dies are formulated in Sec. 2. For the first system the total shear stress

is decomposed into a polymer contribution, evolving in accordance with a differential constitutive relation with a single relaxation time, and a Newtonian viscosity contribution [system (JSO) in Sec. 2]. The second system is based on a differential constitutive law with two widely spaced relaxation times but no Newtonian viscosity [system (JSO_2) in Sec. 2]. We shall show that the dynamics of these two models is similar; this suggests that the qualitative behavior we find is not special to the particular viscoelastic models we have analyzed.

For the highly elastic and very viscous polyisoprenes used in the spurt experiment, the ratio α of Reynolds number to Deborah number is several orders of magnitude smaller than the ratio ε of Newtonian viscosity to shear viscosity. This implies that the flow equations (JSO) are approximated, at each fixed position x in the channel, by the following dynamical system [11]:

$$\begin{aligned} \dot{\sigma} &= (Z+1)\left(\frac{\overline{T}-\sigma}{\varepsilon}\right) - \sigma \,, \\ \dot{Z} &= -\sigma\left(\frac{\overline{T}-\sigma}{\varepsilon}\right) - Z \,. \end{aligned} \tag{1.1}$$

Here the dot denotes the time derivative and $\overline{T} = \overline{f}x$, with $\overline{f}$ being the driving pressure gradient.

Although it has not been proved mathematically that solutions of system (1.1) approximate solutions of (JSO), this conclusion is reinforced by some analytical results as well as by numerical experiments. Nohel, Pego and Tzavaras [13] established that discontinous steady states are stable in a simple model in which the polymer shear stress satisfies a single differential constitutive relation; this model can be arranged to have the same behavior in steady shear as system (JSO). Research in progress suggests that this is true also of the full systems (JSO) and (JSO_2), at least when α is sufficiently small.

Analysis of system (1.1) is carried out in Sec. 3. We show that steady states of system (JSO), some of which are discontinuous, correspond to families of critical points of the dynamical system. We deduce the local characters of the critical points, and prove that the system has no periodic orbits or closed separatrix cycles. Moreover we determine the global dynamics completely through a phase-plane analysis; this is accomplished by constructing a natural Lyapunov-like function. Thus we identify the globally asymptotically stable steady states for each position x.

The same approximation in the model (JSO_2) leads to the study a similar but more complicated dynamical system. In Sec. 4 we show that, in the relevant range of parameters, the essential dynamical features of the latter system are qualitatively the same as those of system (1.1).

In Sec. 5 the results of Secs. 3 and 4 is applied to explain spurt, shape memory, hysteresis, and other effects observed in the numerical simulations. This involves understanding how the phase portraits of system (1.1) change as $\overline{T}$ is varied. In Sec. 6 we develop asymptotic expansions in powers of ε of solutions of the dynamical systems; this enables us to explain the latency effect (a pseudo-steady state that precedes spurt). The asymptotic analysis also permits a more quantitative comparison of the dynamics of the two constitutive models when ε is sufficiently small. In Sec. 7 we discuss physical implications of our

results, particularly those predictions that warrant testing by rheological experiment.

Finally, in Sec. 8, we draw certain conclusions: although the analysis in this paper applies only to the special constitutive models we have studied, we expect that the qualitative features of our results appear in a broad class of non-Newtonian fluids. Indeed, numerical simulation by Kolkka and Ierley [10] shows that another model with a single relaxation time and Newtonian viscosity exhibits similar character.

2. Mathematical Formulation of Generalized Johnson-Segalman Models

The motion of a fluid under incompressible and isothermal conditions is governed by the balance of linear momentum

$$\rho \left[\frac{\partial \mathbf{v}}{\partial t} + \mathbf{v} \cdot \nabla \mathbf{v} \right] = \nabla \cdot \mathbf{S} \ . \tag{2.1}$$

Here ρ is the fluid density, $\mathbf{v}$ is the particle velocity, and $\mathbf{S}$ is the total stress tensor. The response characteristics of the fluid are embodied in the constitutive relation for the stress. For viscoelastic fluids with fading memory, these relations specify the stress as a functional of the deformation history of the fluid. Many sophisticated constitutive models have been devised; see Ref. [2] for a survey. In the present work, we focus on a class of multi-mode differential models. These models generalize the Johnson-Segalman model [8] by allowing for a distinct slip parameter for each mode; alternatively, one can regard each mode to be governed by a special case of the Oldroyd constitutive equation [14]. As discussed in Secs. 1 and 8, we believe that qualitative aspects of our results are not limited to these particular models.

To specify these constitutive relations, we decompose the total stress as

$$\mathbf{S} = -p\mathbf{I} + 2\eta\mathbf{D} + \mathbf{\Pi} \ . \tag{2.2}$$

In this equation, p is an isotropic pressure (which is determined from the incompressibility constraint) and η is the coefficient of Newtonian viscosity; we let $\mathbf{D} := \frac{1}{2}\left[\nabla\mathbf{v} + (\nabla\mathbf{v})^T\right]$ and $\mathbf{\Omega} := \frac{1}{2}\left[\nabla\mathbf{v} - (\nabla\mathbf{v})^T\right]$ be the symmetric and antisymmetric parts of the velocity gradient $\nabla\mathbf{v}$, which has components $(\nabla\mathbf{v})^i{}_j := \partial v^i/\partial x^j$. The tensor $\mathbf{\Pi}$ is the non-Newtonian extra stress, which we decompose into partial stresses:

$$\mathbf{\Pi} := \sum_{j=1}^{m} \boldsymbol{\pi}_j \ . \tag{2.3}$$

Each partial stress $\boldsymbol{\pi}_j$ is specified by the differential constitutive law

$$\overset{*}{\boldsymbol{\pi}}_j = 2\mu_j\mathbf{D} - \lambda_j\boldsymbol{\pi}_j \ , \tag{2.4}$$

where

$$\overset{*}{\boldsymbol{\pi}}_j := \frac{\partial \boldsymbol{\pi}_j}{\partial t} + (\mathbf{v}\cdot\nabla)\,\boldsymbol{\pi}_j - \boldsymbol{\pi}_j\nabla\mathbf{v} - (\nabla\mathbf{v})^T\,\boldsymbol{\pi}_j + (1-a_j)\,(\boldsymbol{\pi}_j\mathbf{D} + \mathbf{D}\boldsymbol{\pi}_j) \tag{2.5}$$

is the objective time derivative of $\boldsymbol{\pi}_j$ with slip parameter a_j. The parameters μ_j are elastic shear moduli, and the λ_j are relaxation rates; the quotients μ_j/λ_j are shear viscosities.

Essential properties of constitutive relations are exhibited in simple planar Poiseuille shear flow. With the flow aligned along the y-axis (see Fig. 1), the flow variables are independent of y. Therefore the velocity field is $\mathbf{v} = (0, v(x,t))$, and the balance of mass is automatically satisfied. Furthermore, the components of each partial stress tensor $\boldsymbol{\pi}_j$ can be written $\boldsymbol{\pi}_j^{xx} = \gamma_j(x,t)$, $\boldsymbol{\pi}_j^{xy} = \boldsymbol{\pi}_j^{yx} = \sigma_j(x,t)$, and $\boldsymbol{\pi}_j^{yy} = \tau_j(x,t)$, while the pressure takes the form $p = p_0(x,t) - f(t)y$, f being the pressure gradient driving the flow. In these terms, Eqs. (2.4) become

$$\begin{aligned} &\gamma_{jt} + (1-a_j)\sigma_j v_x = -\lambda_j \gamma_j \ , \\ &\sigma_{jt} - \left[\tfrac{1}{2}(1+a_j)\gamma_j - \tfrac{1}{2}(1-a_j)\tau_j + \mu_j\right] v_x = -\lambda_j \sigma_j \ , \\ &\tau_{jt} - (1+a_j)\sigma_j v_x = -\lambda_j \tau_j \ . \end{aligned} \tag{2.6}$$

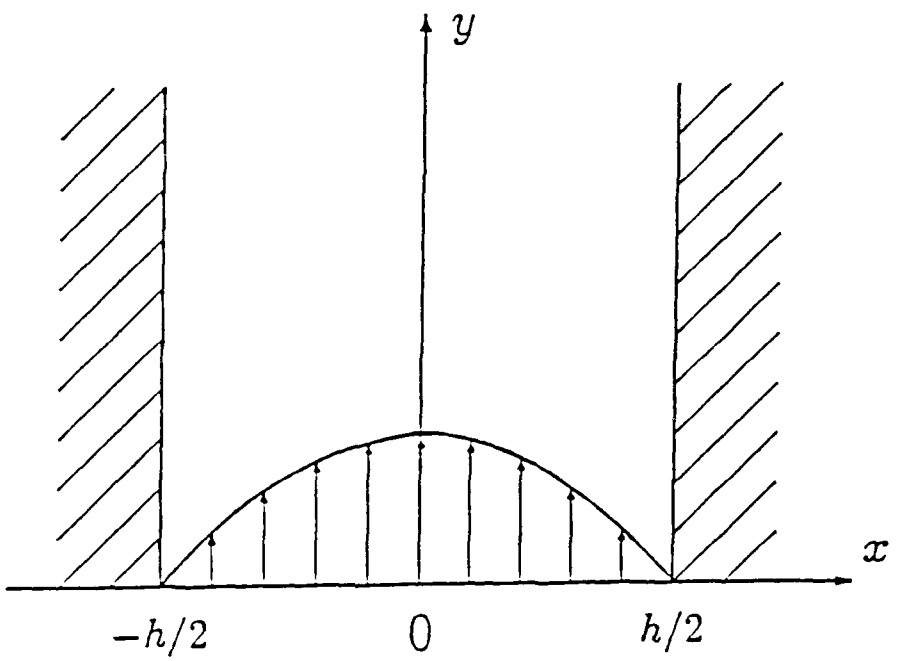

Fig. 1: Shear flow through a slit-die.

For each j, we introduce the variables

$$Z_j := \tfrac{1}{2}(1+a_j)\gamma_j - \tfrac{1}{2}(1-a_j)\tau_j \tag{2.7}$$

and

$$W_j := -\tfrac{1}{2}(1+a_j)\gamma_j - \tfrac{1}{2}(1-a_j)\tau_j \ . \tag{2.8}$$

Taking linear combinations of the first and last of Eqs. (2.6) yields an equivalent pair of equations for Z_j and W_j. The equation for W_j is $W_{jt} = -\lambda_j W_j$; noting that W_j must remain finite as $t \to -\infty$, we conclude that $W_j \equiv 0$. Thus the two evolution equations for γ_j and τ_j can be replaced by a single equation for Z_j. Furthermore, $Z_j = -\frac{1}{2}(1-a_j^2)(\tau_j - \gamma_j)$, so that Z_j represents a contribution to the principal normal stress difference, $\sum_{j=1}^m \left(\boldsymbol{\pi}_j^{yy} - \boldsymbol{\pi}_j^{xx}\right) = \sum_{j=1}^m (\tau_j - \gamma_j)$.

With these observations, Eqs. (2.6), combined with the balance of linear momentum, Eq. (2.1), reduce to

$$\begin{aligned} &\rho v_t - \sum_{j=1}^m \sigma_{jx} = \eta v_{xx} + f \ , \\ &\sigma_{jt} - (Z_j + \mu_j)\, v_x = -\lambda_j \sigma_j \ , \\ &Z_{jt} + \left(1 - a_j^2\right) \sigma_j v_x = -\lambda_j Z_j \ . \end{aligned} \tag{2.9}$$

This system serves as a basis for the flow problems discussed below. For later reference, notice that the momentum equation in Eq. (2.9) can be written as $\rho v_t - T_x = f$, where

$$T := \sum_{j=1}^m \sigma_j + \eta v_x \tag{2.10}$$

is the total shear stress. If $\eta = 0$, it is readily shown that system (2.9) is hyperbolic if $\sum_{j=1}^m (Z_j + \mu_j) \geq 0$, with wave speeds $\pm \left[\rho^{-1} \sum_{j=1}^m (Z_j + \mu_j)^{1/2}\right]$ and 0 (repeated $2m-1$ times). Moreover, for initial-boundary-value problems appropriate for shear flow, and for smooth data compatible with the boundary conditions, techniques in Ref. [16] can be used to establish global well-posedness of classical solutions if the data have small total variation, and finite-time blow-up of classical solutions if the data have large variation.

If $\eta > 0$, general theory developed in Ref. [13, Sec. 3 and App. A] yields global existence of classical solutions for smooth initial data of arbitrary size, and also existence of almost classical, strong solutions with discontinuities in the initial velocity gradient and in the stress components; the latter result allows one to prescribe discontinuous initial data of the same type as the discontinuous steady states studied in this paper.

In what follows, we will consider two special cases: (A) the case of a single relaxation time ($m = 1$) in the presence of Newtonian viscosity ($\eta \neq 0$); and (B) the case of two relaxation times ($m = 2$) but no Newtonian viscosity ($\eta = 0$). The study of these two models determines how the effect of Newtonian viscosity compares to the effect of a second relaxation time. In both cases we study the Poiseuille shear flow between parallel plates located at $x = \pm h/2$ (*cf.* Fig. 1).

A. Single Relaxation Time. To simplify notation, we omit the subscript j, and we nondimensionalize the variables by scaling distance by h, time by λ^{-1}, and stress by μ. Furthermore, if we replace σ, v, and f by $\hat{\sigma} := (1-a^2)^{1/2}\sigma$, $\hat{v} := (1-a^2)^{1/2}v$, and $\hat{f} := (1-a^2)^{1/2}f$, respectively, then the parameter a disappears from Eqs. (2.9). Since no confusion will arise, we omit the caret. There are two essential dimensionless parameters:

$$\alpha := \rho h^2 \lambda^2 / \mu \ , \tag{2.11}$$

a ratio of Reynolds number to Deborah number; and

$$\varepsilon := \eta \lambda / \mu \ , \tag{2.12}$$

a ratio of viscosities.

The resulting initial–boundary-value problem governing the flow [11] is the system

$$\begin{aligned} &\alpha v_t - \sigma_x = \varepsilon v_{xx} + f \ , \\ &\sigma_t - (Z+1)v_x = -\sigma \ , \\ &Z_t + \sigma v_x = -Z \end{aligned} \tag{JSO}$$

on the interval $[-1/2, 0]$, with boundary conditions

$$v(-1/2, t) = 0 \quad \text{and} \quad v_x(0,t) = 0 \tag{BC}$$

and initial conditions

$$v(x,0) = v_0(x) \ , \quad \sigma(x,0) = \sigma_0(x) \ , \quad \text{and} \quad Z(x,0) = Z_0(x) \ , \tag{IC}$$

where $v_0(-1/2) = 0$, $v_0'(0) = 0$ and $\sigma_0(0) = 0$. When $\varepsilon = 0$, and $Z + 1 \geq 0$, the system is hyperbolic, with characteristics speeds 0 and $\pm[(Z+1)/\alpha]^{1/2}$ and 0.

The steady-state solutions of system (JSO), when the forcing term f is a constant $\overline{f}$, play an important role in our discussion. Such a solution, denoted by $\overline{v}$, $\overline{\sigma}$, and $\overline{Z}$, can be described as follows. The stress components $\overline{\sigma}$ and $\overline{Z}$ are related to the strain rate $\overline{v}_x$ through

$$\overline{\sigma} = \frac{\overline{v}_x}{1 + \overline{v}_x^2} \tag{2.13}$$

and

$$\overline{Z} + 1 = \frac{1}{1 + \overline{v}_x^2} \ . \tag{2.14}$$

Therefore, the steady total shear stress $\overline{T} := \overline{\sigma} + \varepsilon \overline{v}_x$ is given by $\overline{T} = w(\overline{v}_x)$, where

$$w(s) := \frac{s}{1+s^2} + \varepsilon s \ . \tag{2.15}$$

The properties of w, the steady-state relation between shear stress and shear strain rate, are crucial to the behavior of the flow. By symmetry, it suffices to consider $s \geq 0$.

For all $\varepsilon > 0$, the function w has inflection points at $s = 0$ and $s = \sqrt{3}$. When $\varepsilon > 1/8$, the function w is strictly increasing, but when $\varepsilon < 1/8$, the function w is not monotone. Lack of monotonicity is the fundamental cause of the non-Newtonian behavior studied in this paper, so hereafter we assume that $\varepsilon < 1/8$.

The graph of w is shown in Fig. 2. Specifically, w has a maximum at $s = s_M$ and a minimum at $s = s_m$, where

$$s_M, s_m = \left[\frac{1 - 2\varepsilon \mp \sqrt{1 - 8\varepsilon}}{2\varepsilon}\right]^{1/2} , \tag{2.16}$$

respectively, at which points it takes the values $\overline{T}_M := w(s_M)$ and $\overline{T}_m := w(s_m)$. The function w has an inflection point at $s_{\text{infl}} = \sqrt{3}$. As $\varepsilon \to 1/8$ from below, the two extrema of w coalesce at s_{infl}. Another limit, $\varepsilon \to 0$, occurs in applications to rheological experiments (see Sec. 6); in this vein, we record the following asymptotic formulae:

$$s_M = 1 + 2\varepsilon + 6\varepsilon^2 + O(\varepsilon^3) , \tag{2.17}$$

$$\overline{T}_M = 1/2 + \varepsilon + \varepsilon^2 + O(\varepsilon^3) , \tag{2.18}$$

$$s_m = \varepsilon^{-1/2}[1 - (3/2)\varepsilon - (25/8)\varepsilon^2 + O(\varepsilon^3)] , \tag{2.19}$$

$$\overline{T}_m = \varepsilon^{1/2}[2 - \varepsilon - (5/4)\varepsilon^2 + O(\varepsilon^3)] . \tag{2.20}$$

The momentum equation, together with the boundary condition at the centerline, implies that the steady total shear stress satisfies $\overline{T} = -\overline{f}x$ for every $x \in [-\frac{1}{2}, 0]$. Therefore, the steady velocity gradient can be determined as a function of x by solving

$$w(\overline{v}_x) = -\overline{f}x . \tag{2.21}$$

Equivalently, a steady state solution $\overline{v}_x$ satisfies the cubic equation $P(\overline{v}_x) = 0$, where

$$P(s) := \varepsilon s^3 - \overline{T}s^2 + (1 + \varepsilon)s - \overline{T} . \tag{2.22}$$

The steady velocity profile in Fig. 3 is obtained by integrating $\overline{v}_x$ and using the boundary condition at the wall. However, because the function w is not monotone, there might be up to three distinct values of $\overline{v}_x$ that satisfy Eq. (2.21) for any particular x on the interval $[-1/2, 0]$. Consequently, $\overline{v}_x$ can suffer jump discontinuities, resulting in kinks in the velocity profile (as at the point x_* in Fig. 3). Indeed, a steady solution must contain such a jump if the total stress $\overline{T}_{\text{wall}} = \overline{f}/2$ at the wall exceeds the total stress $\overline{T}_M$ at the local maximum M in Fig. 2.

Let us describe in more detail the analytical solutions for steady flow fields in two instances: subcritical flow (having no kinks) and supercritical flow with one kink (as is pictured in Fig. 3). To this end, it is useful to define $s_{\text{sup}}(T)$ for $\overline{T}_m \le T$ and $T \le -\overline{T}_m$ to be the root s of $w(s) = T$ with largest absolute value, while $s_{\text{sub}}(T)$ for $-\overline{T}_M \le T \le \overline{T}_M$ is the root with smallest absolute value. Then we define the following antiderivatives:

$$\begin{aligned} V_{\text{sup}}(x) &:= \overline{f}^{-1} \int^{-\overline{f}x} s_{\text{sup}}(T)\, dT , \\ V_{\text{sub}}(x) &:= \overline{f}^{-1} \int^{-\overline{f}x} s_{\text{sub}}(T)\, dT . \end{aligned} \tag{2.23}$$

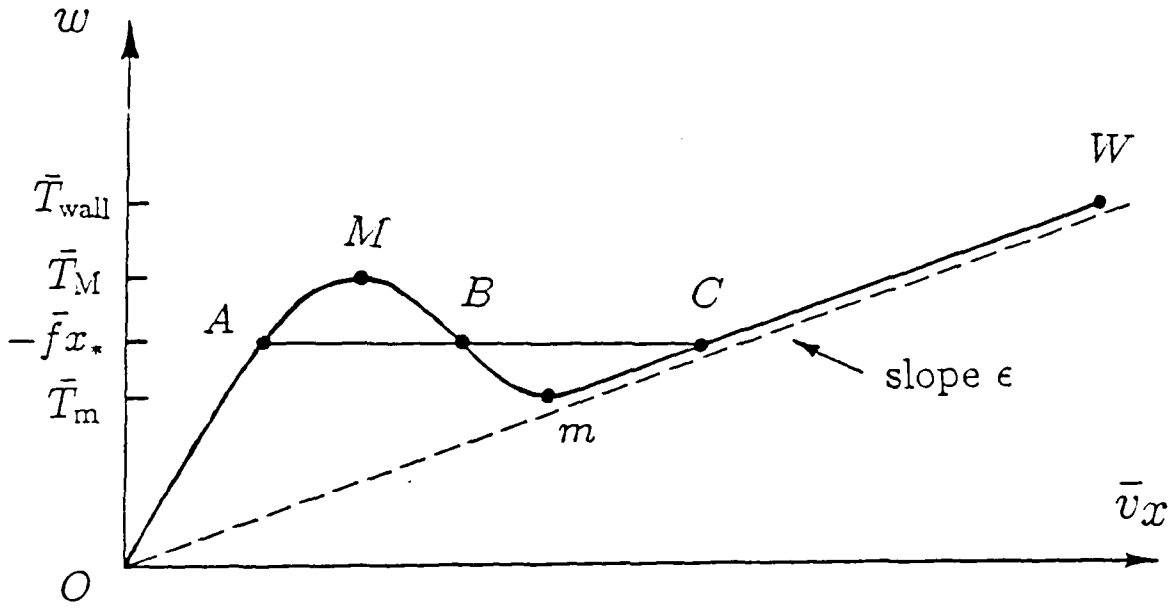

Fig. 2: Total steady shear stress $\overline{T}$ *vs.* shear strain rate $\overline{v}_x$ for steady flow. The case of three critical points is illustrated; other possibilities are discussed in Sec. 3.

Because $\overline{T}(x) = -\overline{f}x$, the steady velocity field is given as follows:

subcritical flow:

$$\overline{v}(x) = V_{\rm sub}(x) - V_{\rm sub}(-1/2) \; ; \tag{2.24}$$

supercritical flow:

$$\overline{v}(x) = \begin{cases} V_{\rm sup}(x) - V_{\rm sup}(-1/2) \; , & x \le x_* \; , \\ V_{\rm sup}(x_*) + V_{\rm sub}(x) - V_{\rm sub}(x_*) \; , & x > x_* \; , \end{cases} \tag{2.25}$$

where x_* is the location of the jump in $\overline{v}_x$, which is related to the stress $\overline{T}_*$ at the discontinuity by

$$x_* = -\tfrac{1}{2}\overline{T}_*/\overline{T}_{\rm wall} \; . \tag{2.26}$$

Determination of x_* and $\overline{T}_*$ from the system dynamics is discussed in Sec. 6. Integrating the velocity with respect to x yields the flow rate per cross-section

$$Q := 2\int_{-1/2}^{0} \overline{v}(x)\, dx \; . \tag{2.27}$$

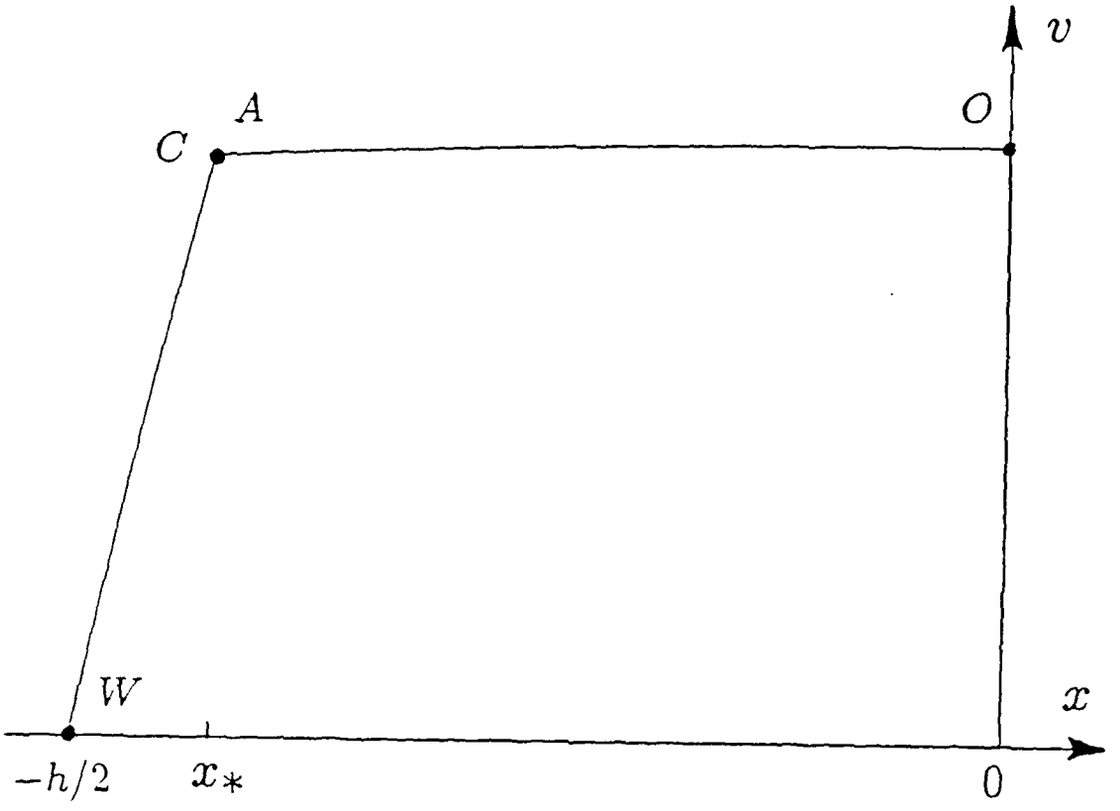

Fig. 3: Velocity profile for steady flow.

This quantity is the one most easily observed experimentally and, along with $\overline{T}_{\text{wall}}$, is the primary datum describing the spurt phenomenon reported by Vinogradov *et al.* [17].

This approach to obtaining analytical steady flows, if applied directly using the cubic formula, yields an expression for $\overline{v}$ that is intractable. An alternate approach is to integrate the asymptotic expression for $\overline{v}_x$ that is obtained in Sec. 6. This is straight-forward and results in a fairly compact closed-form formula [18]. On the other hand, changing variables of integration from from shear stress to strain rate in Eqs. (2.23), yields integrals that can be evaluated explicitly; we refer to Ref. [18] for details of this development.

B. Two Relaxation Times. By analogy with the previous model, we nondimensionalize the variables by scaling distance by h, time by λ_1^{-1}, and stress by μ_1; also, we replace σ_j, v, and f by $\hat{\sigma}_j := (1-a_1^2)^{1/2}\sigma_j$, $\hat{v} := (1-a_1^2)^{1/2}v$, and $\hat{f} := (1-a_1^2)^{1/2}f$, respectively, and we omit the caret. It proves convenient to choose dimensionless variables as follows:

$$\alpha := \rho h^2 \lambda_1^2/\mu_1 \,, \tag{2.28}$$

$$\beta := \mu_2/\mu_1 \,, \tag{2.29}$$

$$\delta := (1-a_2^2)/(1-a_1^2) \,, \tag{2.30}$$

$$\kappa := \lambda_1\mu_2/(\lambda_2\mu_1) \,, \tag{2.31}$$

In this notation, the initial–boundary-value problem for the system becomes

$$\begin{aligned} &\alpha v_t - [\sigma_1 + \sigma_2]_x = f \ , \\ &\sigma_{1t} - (Z_1 + 1)v_x = -\sigma_1 \\ &Z_{1t} + \sigma_1 v_x = -Z_1 \ , \\ &\sigma_{2t} - (Z_2 + \beta)v_x = -\kappa^{-1}\beta\sigma_2 \ , \\ &Z_{2t} + \delta\sigma_2 v_x = -\kappa^{-1}\beta Z_2 \end{aligned} \qquad (JSO_2)$$

on the interval $[-1/2, 0]$, with boundary conditions (BC) and initial conditions $v(x,0) = v_0(x)$ and

$$\sigma_j(x,0) = \sigma_{0j}(x) \quad \text{and} \quad Z_j(x,0) = Z_{0j}(x) \ , \qquad (IC_j)$$

where $j = 1, 2$; again we require that $v_0(-1/2) = 0$, $v_0'(0) = 0$, and $\sigma_{0j}(0) = 0$. The condition for hyperbolicity of system (JSO_2) is $Z_1 + 1 + Z_2 + \beta \geq 0$, in which case the characteristics speeds are 0 (repeated three times) and $\pm[(Z_1 + 1 + Z_2 + \beta)/\alpha]^{1/2}$.

The steady-state solutions of system (JSO_2) are given by

$$\begin{aligned} \overline{\sigma}_1 &= \frac{\overline{v}_x}{1 + \overline{v}_x^2} \ , \\ \overline{\sigma}_2 &= \frac{\kappa\overline{v}_x}{1 + \delta\kappa^2\beta^{-2}\overline{v}_x^2} \ , \end{aligned} \qquad (2.32)$$

and

$$\begin{aligned} \overline{Z}_1 + 1 &= \frac{1}{1 + \overline{v}_x^2} \\ \overline{Z}_2 + \beta &= \frac{\beta}{1 + \delta\kappa^2\beta^{-2}\overline{v}_x^2} \ . \end{aligned} \qquad (2.33)$$

Again, the steady total shear stress $\overline{T} = \overline{\sigma}_1 + \overline{\sigma}_2$ satisfies $\overline{T} = -\overline{f}x$; thus the steady state solution $\overline{v}_x$ satisfies the quartic equation $P_2(\overline{v}_x) = 0$, where

$$P_2(s) := -\overline{T}\delta\kappa^2\beta^{-2}s^4 + (\kappa + \delta\kappa^2\beta^{-2})s^3 - \overline{T}(1 + \delta\kappa^2\beta^{-2})s^2 + (1 + \kappa)s - \overline{T} \ . \qquad (2.34)$$

We note that if $\delta = 0$ and $\kappa = \varepsilon$, then $P_2 = P$, and the steady states of system (JSO_2) and of system (JSO) coincide.

3. Phase Plane Analysis for System (JSO) When $\alpha = 0$

A great deal of information about the structure of solutions of system (JSO) can be garnered by studying a system of ordinary differential equations that approximates it in a certain parameter range. Motivation for this approximation comes from the following observation: in experiments of Vinogradov *et al.* [17], $\alpha = \rho h^2 \lambda^2 / \mu$ is of the order 10^{-12}; thus the term αv_t in the momentum equation of system (JSO) is negligible even when v_t is moderately large. We are led to study the approximation to system (JSO) obtained when $\alpha = 0$. The behavior of solutions of the resulting dynamical system offers an explanation for several features of the solutions of the full system (JSO) observed in the computations of Refs. [9, 11]; in fact, these calculations prompted the following analysis, which determines the dynamics of the approximating system completely.

When $\alpha = 0$, the momentum equation in system (JSO) can be integrated, just as in the case of steady flows, to show that the total shear stress $T := \sigma + \varepsilon v_x$ coincides with the steady value $\overline{T}(x) = -\overline{f}x$. Thus $T = \overline{T}(x)$ is a function of x only, even though σ and v_x are functions of both x and t. The remaining equations of system (JSO) yield, for each fixed x, the autonomous, quadratic, planar system of ordinary differential equations

$$\begin{aligned} \dot{\sigma} &= (Z+1)\left(\frac{\overline{T}-\sigma}{\varepsilon}\right) - \sigma \,, \\ \dot{Z} &= -\sigma\left(\frac{\overline{T}-\sigma}{\varepsilon}\right) - Z \,. \end{aligned} \tag{3.1}$$

Here the dot denotes the derivative d/dt. We emphasize that for each $\overline{f}$, a different dynamical system is obtained at each x on the interval $[-1/2, 0]$ in the channel because $\overline{T} = -\overline{f}x$. By symmetry, we may focus attention on the case $\overline{T} > 0$; this is assumed throughout Secs. 3 and 4. The dynamical system (3.1) can be analyzed completely by a phase-plane analysis, which we carry out in detail. Recall from Sec. 2 that we assume $\varepsilon < 1/8$ throughout.

The critical points of system (3.1) satisfy the algebraic system

$$\begin{aligned} &(Z+1+\varepsilon)\left(\frac{\sigma}{\overline{T}} - 1\right) + \varepsilon = 0 \,, \\ &\frac{\overline{T}^2}{\varepsilon}\frac{\sigma}{\overline{T}}\left(\frac{\sigma}{\overline{T}} - 1\right) - Z = 0 \,. \end{aligned} \tag{3.2}$$

These equations define, respectively, a hyperbola and a parabola in the σ-Z plane; these curves are drawn in Fig. 4, which corresponds to the most comprehensive case of three critical points. The critical points are intersections of these curves. In particular, critical points lie in the strip $0 < \sigma < \overline{T}$.

Eliminating Z in these equations shows that the σ-coordinates of the critical points satisfy the cubic equation $Q(\sigma/\overline{T}) = 0$, where

$$Q(\xi) := \left[\frac{\overline{T}^2}{\varepsilon}\xi(\xi-1) + 1 + \varepsilon\right](\xi - 1) + \varepsilon \,. \tag{3.3}$$

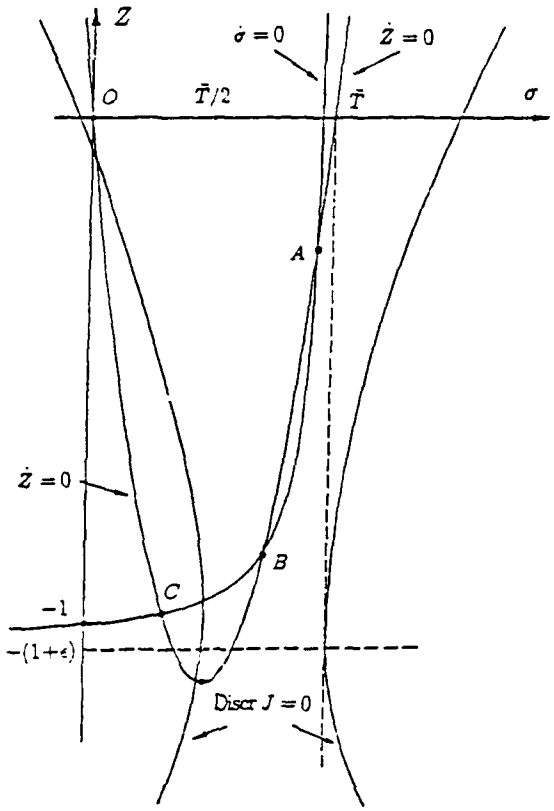

Fig. 4: The phase plane in the case of three critical points.

A straightforward calculation using Eq. (2.22) shows that

$$P(\overline{v}_x) = P\left(\frac{\overline{T}-\sigma}{\varepsilon}\right) = -\frac{\overline{T}}{\varepsilon}Q(\sigma/\overline{T}) \; . \tag{3.4}$$

Thus each critical point of the system (3.1) defines a steady-state solution of system (JSO): such a solution corresponds to a point on the steady total-stress curve (see Fig. 2) at which the total stress is $\overline{T}(x)$. Depending on the value of $\overline{T}$, and hence x, there are either one, two, or three critical points. To simplify the ensuing discussion, we shall ignore the degenerate cases of two critical points, where $\overline{T} = \overline{T}_M$ or $\overline{T} = \overline{T}_m$. Consequently, we have:

Proposition 3.1: *For (almost) all positions x in the channel, there are three possibilities:*
(1) there is a single critical point A when $\overline{T}(x) < \overline{T}_m$;
(2) there is a single critical point C when $\overline{T}(x) > \overline{T}_M$;
(3) there are three critical points A, B, and C, with $\sigma_A > \sigma_B > \sigma_C$, when $\overline{T}_m < \overline{T}(x) < \overline{T}_M$.

To determine the qualitative structure of the dynamical system (3.1), we first study the nature of the critical points. The behavior of orbits near a critical point depends on

the linearization of Eq. (3.1) at this point, *i.e.*, on the eigenvalues of the Jacobian

$$\mathbf{J} = \begin{pmatrix} -\frac{1}{\varepsilon}(Z+1+\varepsilon) & -\frac{\overline{T}}{\varepsilon}\left(\frac{\sigma}{\overline{T}}-1\right) \\ \frac{\overline{T}}{\varepsilon}\left(2\frac{\sigma}{\overline{T}}-1\right) & -1 \end{pmatrix} , \tag{3.5}$$

evaluated at the critical point. The character of the eigenvalues of $\mathbf{J}$ can be determined from the signs of the trace of $\mathbf{J}$, given by

$$-\varepsilon \,\mathrm{Tr}\,\mathbf{J} = Z + 1 + 2\varepsilon \; ; \tag{3.6}$$

the determinant of $\mathbf{J}$, given by

$$\varepsilon \,\mathrm{Det}\,\mathbf{J} = Z + 1 + \varepsilon + \frac{\overline{T}^2}{\varepsilon}\left(2\frac{\sigma}{\overline{T}}-1\right)\left(\frac{\sigma}{\overline{T}}-1\right) \; ; \tag{3.7}$$

and the discriminant of $\mathbf{J}$, given by

$$\varepsilon^2 \,\mathrm{Discrm}\,\mathbf{J} = (Z+1)^2 - 8\overline{T}^2\left(\frac{\sigma}{\overline{T}}-\frac{3}{4}\right)^2 + \tfrac{1}{2}\overline{T}^2 \; . \tag{3.8}$$

We note a useful fact: at a critical point,

$$\varepsilon \,\mathrm{Det}\,\mathbf{J} = Q'(\sigma/\overline{T}) \; ; \tag{3.9}$$

this follows by using the second of Eqs. (3.2) to replace Z in Eq. (3.7). This relation is important because Q' is positive at A and C and negative at B.

The character of the eigenvalues can be understood using these formulae together with Fig. 4. In addition to the hyperbola on which $\dot{\sigma} = 0$ and the parabola on which $\dot{Z} = 0$ [see Eqs. (3.2)], Fig. 4 shows the hyperbola on which $\mathrm{Discrm}\,\mathbf{J}$ vanishes [see Eq. (3.8)]. We draw the following conclusions:

(1) $\mathrm{Tr}\,\mathbf{J} < 0$ at all critical points;
(2) $\mathrm{Det}\,\mathbf{J} > 0$ at A and C, while $\mathrm{Det}\,\mathbf{J} < 0$ at B; and
(3) $\mathrm{Discrm}\,\mathbf{J} > 0$ at A and B, whereas $\mathrm{Discrm}\,\mathbf{J}$ can be of either sign at C. (For "most" values of ε and $\overline{T}$, $\mathrm{Discrm}\,\mathbf{J} < 0$ at C; in particular, $\mathrm{Discrm}\,\mathbf{J} < 0$ if C is the only critical point. But it is possible for $\mathrm{Discrm}\,\mathbf{J}$ to be positive if $\overline{T}$ is sufficiently close to $\overline{T}_m$.)

Standard theory of nonlinear planar dynamical systems (see, *e.g.*, Ref. [3, Chap. 15]) now establishes the local characters of the critical points A, B, and C in Prop. 3.1:

Proposition 3.2:
(1) A is an attracting node (called the classical attractor);
(2) B is a saddle point;
(3) C is either an attracting spiral point or an attracting node (called the spurt attractor).

The next task is to determine the global structure of the orbits of system (3.1). In this direction, we employ an argument based on a suggestion by A. Coppel [4].

Proposition 3.3: *System (3.1) has neither periodic orbits nor separatrix cycles.*

For the proof, notice that $\dot{\sigma} = -\sigma \neq 0$ along the line $\sigma = \overline{T}$, so that no periodic orbit can cross this line. Since all critical points lie in the half-plane $\sigma < \overline{T}$, any periodic orbit (which must surround some critical point, by the Poincaré-Bendixson theorem) necessarily lies in this half plane. Let the scaled time variable s be defined by $ds = (\overline{T} - \sigma)\, dt$; then with a prime denoting differentiation with respect to s, system (3.1) transforms to

$$\begin{aligned} \sigma' &= \varepsilon^{-1}(Z+1) - \sigma/(\overline{T} - \sigma) =: p(\sigma, Z) \ , \\ Z' &= -\varepsilon^{-1}\sigma - Z/(\overline{T} - \sigma) =: q(\sigma, Z) \ . \end{aligned} \tag{3.10}$$

Since

$$\partial p/\partial \sigma + \partial q/\partial Z = -(2\overline{T} - \sigma)/(\overline{T} - \sigma)^2 \ , \tag{3.11}$$

is strictly negative for $\sigma < \overline{T}$, existence of periodic orbits and separatrix cycles is excluded by Bendixson's criterion [1].

To understand the global qualitative behavior of orbits, we construct suitable invariant sets. In this regard, a crucial tool is the identity

$$\frac{d}{dt}\left\{\sigma^2 + (Z+1)^2\right\} = -2\left[\sigma^2 + (Z + \tfrac{1}{2})^2 - \tfrac{1}{4}\right] \ , \tag{3.12}$$

which is obtained by multiplying the first of Eqs. (3.1) by σ and adding the second, multiplied by $Z + 1$. Thus the function $V(\sigma, Z) := \sigma^2 + (Z+1)^2$ serves as a Lyapunov function for the dynamical system. Notice that identity (3.12) is independent of $\overline{T}$ and ε.

Let Γ denote the circle on which the right side of Eq. (3.12) vanishes. Also let C_r denote the circle of radius r centered at $\sigma = 0$ and $Z = -1$, along which $V(\sigma, Z) = r$; thus each C_r is a level set of V. The circles Γ and C_1 are shown in Fig. 5, which corresponds to the case of a single critical point, namely the spiral point C; and in Fig. 7, which corresponds to the case of three critical points. For later convenience, denote by D the point where C_1 intersects the parabola on which $\dot{Z} = 0$. Also notice that Eq. (3.12) implies that the critical points of system (3.1) lie on Γ.

If $r > 1$, Γ lies strictly inside C_r. Consequently, Eq. (3.12) shows that the dynamical system (3.1) flows inward at points along C_r. Thus the interior of C_r is a positively invariant set for each $r > 1$. Furthermore, the closed disk bounded by C_1, which is the intersection of these sets, is also positively invariant. This establishes:

Proposition 3.4: *Each closed disk bounded by the circle C_r with $r \geq 1$ is a positively invariant set for the system (3.1).*

The above results will be used to determine the global structure of the orbits of system (3.1) and to analyze the stable and unstable manifolds of the saddle point at B.

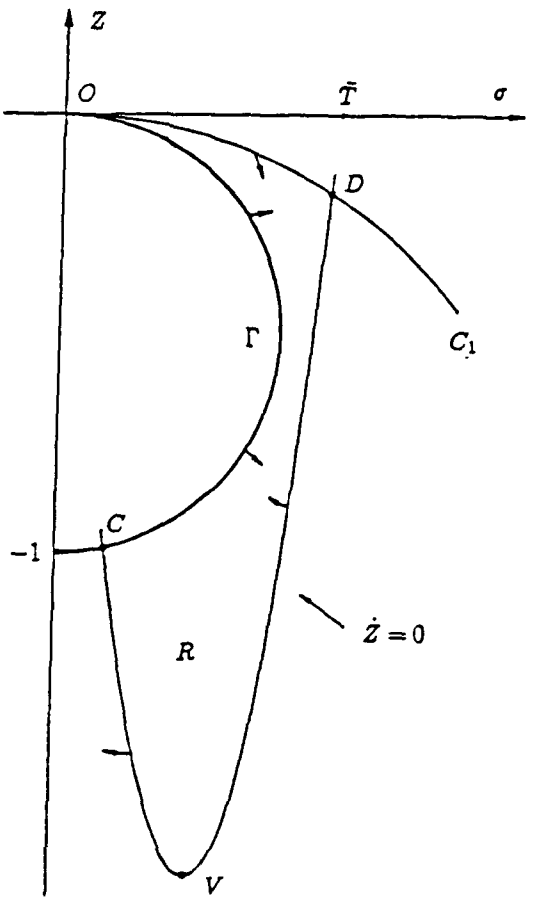

Fig. 5: The phase plane when the spurt attractor $\bar{C}$ is the only critical point.

A. Let us first consider the structure of the flow when there is a single critical point, located at C; see Fig. 5. As shown in Prop. 3.2, the point C must be an attracting spiral point. Because there are no periodic orbits (Prop. 3.3), Prop. 3.4 implies that the orbit through each point in the phase plane tends toward C as t approaches infinity.

In the application to the shear flow problem, we are interested in the particular solution of Eq. (3.1) with initial data $\sigma = 0$ and $Z = 0$ (point O). The orbit of this solution initially remains inside the region $\mathcal{R}$ bounded by $ODVCO$ in Fig. 5, eventually exits through the arc CV of the parabola, and finally spirals toward C. Indeed, the flow is directed into $\mathcal{R}$ along OD (where $\dot{V} \leq 0$), DV (where $\dot{Z} = 0$ and $\dot{\sigma} < 0$), and CO (where $\dot{V} = 0$ and $\dot{\sigma} \geq 0$). Therefore the orbit through O must leave $\mathcal{R}$ along the arc VC of the parabola, whereupon it spirals into C. This solution is illustrated in Fig. 6; note that this solution does not tend to a periodic orbit, according to Prop. 3.3.

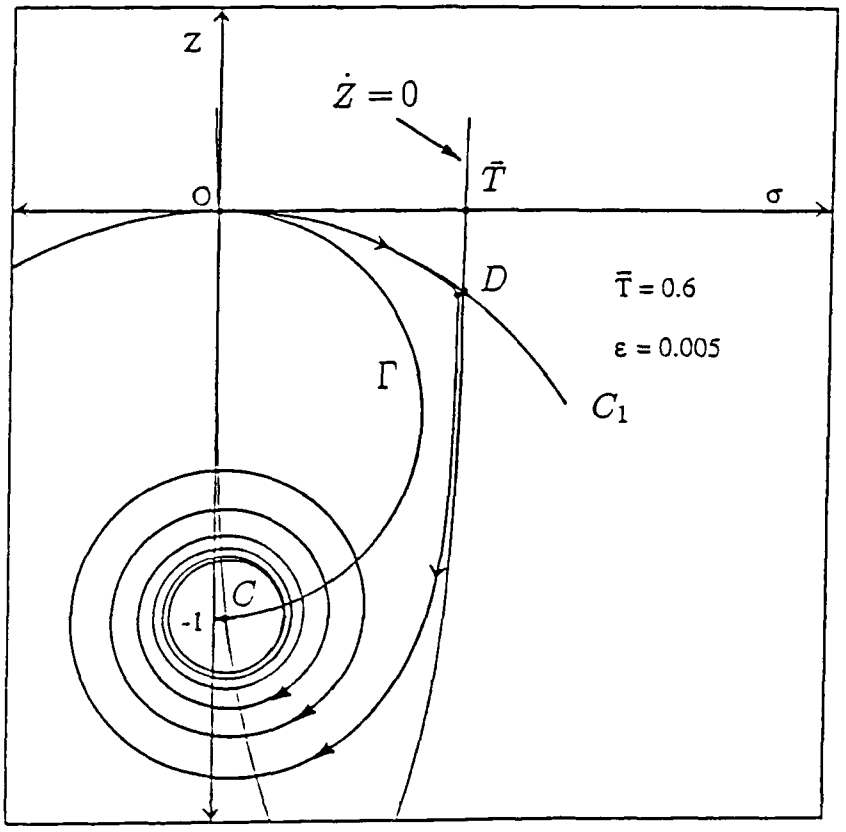

Fig. 6: The orbit through origin when the spurt attractor C is the only critical point.

B. Next, consider the case when there are three critical points, illustrated in Fig. 7. By Prop. 3.3, there are no periodic orbits or closed separatrix cycles. Propositions 3.2 and 3.4 imply that the orbit through any point in the plane either: tends to A; tends to C; or tends to B along its stable manifold as t approaches infinity.

For a more detailed analysis, we first prove that the closed set $\mathcal{I}$ bounded by the curved triangle ODA in Fig. 7 is positively invariant with respect to Eqs. (3.1). This is because the flow is directed into $\mathcal{I}$ along OD (where $\dot{V} \leq 0$), DA (where $\dot{Z} = 0$ and $\dot{\sigma} \leq 0$), and AO (where $\dot{V} = 0$ and $\dot{\sigma} \geq 0$). One consequence of the invariance of $\mathcal{I}$ is that the orbit of the solution of Eq. (3.1) with initial data $\sigma = 0$ and $Z = 0$ flows into the classical attractor A as t approaches infinity.

The next task is to study the stable manifold for the saddle point B in Fig. 7. Through this point we have drawn the circle C_B centered at $\sigma = 0$ and $Z = -1$, which intersects the parabola at E. Let S denote the closed set bounded by the curved triangle ECB in Fig. 7. At points on its boundary, the flow is directed as follows for increasing t: outward from S along EB because $\dot{V} \geq 0$; outward along CB, where $\dot{V} = 0$ and $\dot{\sigma} \geq 0$; and inward along CE because $\dot{Z} = 0$ and $\dot{\sigma} \geq 0$. As a result, one branch of the stable manifold at B must enter S through the arc EC and remain in S. Furthermore, this branch must have crossed

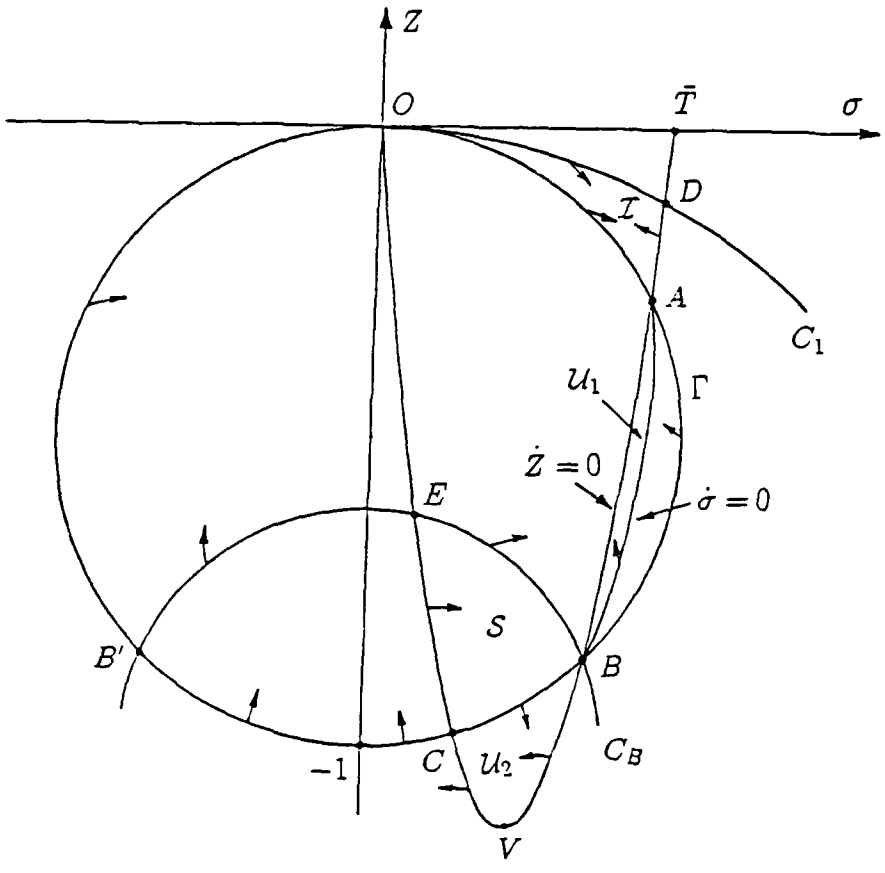

Fig. 7: Invariant regions in the case of three critical points.

the arc CB' of Γ (where B' is the reflection of B about the Z-axis), along which $\dot{V} = 0$ and $\sigma \cdot \dot{\sigma} \leq 0$, because it could not have crossed the arc $B'E$ of C_B. The other branch of the stable manifold enters B through the sector exterior to Γ and the circle C_B. Having come from outside of the circle Γ, where $\dot{V} < 0$, Prop. 3.4 implies that both branches of the stable manifold must have come from infinity in the phase plane.

For the purpose of analyzing the spurt phenomenon in Sec. 5, we summarize these results as follows.

Proposition 3.5: *The basin of attraction of A, i.e., the set of points that flow toward A as $t \to \infty$, comprises those points on the same side of the stable manifold of B as is A; points on the other side are in the basin of attraction of C. Moreover, the arc of the circle Γ through the origin, between B and its reflection B' is contained in the basin of attraction of A.*

To demonstrate the last statement, observe that the flow is directed into the region bounded by the the following curves in Fig. 7: C_1 between O and D; the parabola between D and A; Γ between A and B; C_B between B and B'; and Γ between B' and O. Therefore this region is positively invariant. In particular, the stable manifold for B cannot cross its boundary, so that it cannot cross Γ between B and B'.

Finally, consider the unstable manifold of the saddle point B. Let $\mathcal{U}_1$ be the set

bounded by the arcs of the parabola $\dot{Z} = 0$ and the hyperbola $\dot{\sigma} = 0$ in Fig. 7, between the critical points B and A. Along the open arc of the parabola BA, $\dot{\sigma} > 0$, while along the open arc of the hyperbola, $\dot{Z} > 0$. Therefore, one branch of the unstable manifold at B lies in $\mathcal{U}_1$ and connects B to A. Now consider the set $\mathcal{U}_2$ bounded by BVC, as shown in Fig. 7. The flow is directed into $\mathcal{U}_2$ along BV and CB, so the second branch of the unstable manifold at B remains in $\mathcal{U}_2$ until it exits through the arc VC. If C is a spiral point, this branch enters and leaves $\mathcal{U}_2$ infinitely often as it spirals into C, while if C is an attracting node, it does not reenter $\mathcal{U}_2$ as it tends to C.

To summarize the above description of the dynamics of the system (3.1) with three critical points, the reader is referred to Fig. 8, which shows the case when C is a spiral point.

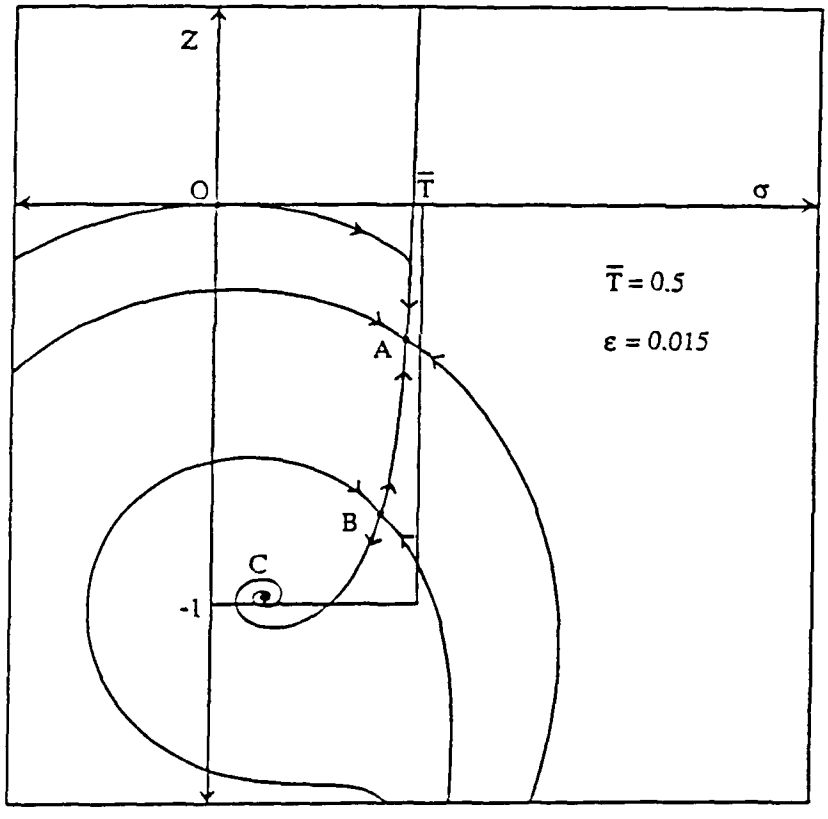

Fig. 8: Phase portrait in the case of three critical points, with C being a spiral.

C. Last is the case of a single critical point at A, which according to Prop. 3.2 is an attracting node. Again, because there are no periodic orbits, Prop. 3.4 implies that all orbits are attracted to A. In particular, the orbit through the origin remains in a region that is analogous to the region $\mathcal{I}$ in Fig. 7.

4. Phase Plane Analysis for a Model with Two Relaxation Times

The purpose of this section is to study the qualitative features of solutions of the system (JSO_2) when $\alpha = 0$. We focus on a special choice for the parameters defining the model: $0 < a_1 < 1$ and $a_2 = 1$ (so that $\delta = 0$). The physical significance of this choice is discussed in Sec. 6. If we identify κ with ε, then the steady states for this model coincide with those of system (JSO) [see Eqs. (2.32)–(2.34)]; again, we assume $\varepsilon < 1/8$. Thus the second relaxation time in system (JSO_2) replaces the Newtonian viscosity in system (JSO), and techniques introduced in Sec. 3 can be applied. The question we address is: to what extent do the dynamics of the present model resemble the dynamics of system (3.1)?

When $\alpha = 0$ and $f = \overline{f}$, the momentum equation in system (JSO_2) can be integrated to show that the total shear stress $T := \sigma_1 + \sigma_2$ equals $\overline{T}(x) = -\overline{f}x$; equivalently, $\dot{\sigma}_1 + \dot{\sigma}_2 = 0$. As a result, adding the stress equations in system (JSO_2) yields

$$(Z_1 + 1 + Z_2 + \beta)\overline{v}_x = \sigma_1 + \varepsilon^{-1}\beta(\overline{T} - \sigma_1) \ . \tag{4.1}$$

Using this equation to eliminate $\overline{v}_x$ leads to an autonomous system of three ordinary differential equations:

$$\begin{aligned}
\dot{\sigma}_1 &= (Z_1 + 1)\frac{\overline{T} - (1 - \varepsilon\beta^{-1})\sigma_1}{\varepsilon\beta^{-1}[Z_1 + 1 + Z_2 + \beta]} - \sigma_1 \ , \\
\dot{Z}_1 &= -\sigma_1\frac{\overline{T} - (1 - \varepsilon\beta^{-1})\sigma_1}{\varepsilon\beta^{-1}[Z_1 + 1 + Z_2 + \beta]} - Z_1 \ , \\
\dot{Z}_2 &= -\delta(T - \sigma_1)\frac{\overline{T} - (1 - \varepsilon\beta^{-1})\sigma_1}{\varepsilon\beta^{-1}[Z_1 + 1 + Z_2 + \beta]} - \varepsilon^{-1}\beta Z_2 \ .
\end{aligned} \tag{4.2}$$

The assumption $\delta = 0$, coupled with the requirement that Z_2 be finite as $t \to -\infty$, shows that $Z_2 \equiv 0$; thus the last of Eqs. (4.2) can be eliminated. Since no confusion will arise by omitting subscripts, we write the dynamical system as

$$\begin{aligned}
\dot{\sigma} &= (Z + 1)\frac{\overline{T} - (1 - \varepsilon\beta^{-1})\sigma}{\varepsilon\beta^{-1}[Z + 1 + \beta]} - \sigma \ , \\
\dot{Z} &= -\sigma\frac{\overline{T} - (1 - \varepsilon\beta^{-1})\sigma}{\varepsilon\beta^{-1}[Z + 1 + \beta]} - Z \ .
\end{aligned} \tag{4.3}$$

Notice that the identity

$$\frac{d}{dt}\left\{\sigma^2 + (Z + 1)^2\right\} = -2\left[\sigma^2 + (Z + \tfrac{1}{2})^2 - \tfrac{1}{4}\right] \tag{4.4}$$

holds for system (4.3) just as it does for system (3.1).

The relationship to system (3.1) is highlighted by scaling the time parameter: define the scaled time s to satisfy $dt = \beta^{-1}[Z + 1 + \beta]\, ds$, and let a prime denote the derivative d/ds. Then

$$\begin{aligned}
\sigma' &= (Z + 1)\left(\frac{\overline{T} - \sigma}{\varepsilon}\right) - \sigma \ , \\
Z' &= -\sigma\left(\frac{\overline{T} - \sigma}{\varepsilon}\right) - Z - \beta^{-1}\left\{\sigma^2 + (Z + \tfrac{1}{2})^2 - \tfrac{1}{4}\right\}
\end{aligned} \tag{4.5}$$

and

$$\frac{d}{ds}\left\{\sigma^2+(Z+1)^2\right\} = -2\beta^{-1}[Z+1+\beta]\left[\sigma^2+(Z+\tfrac{1}{2})^2-\tfrac{1}{4}\right] \ . \tag{4.6}$$

Another useful way of writing system (4.3) is obtained by multiplying Eqs. (4.3) by $\beta^{-1}[Z+1+\beta]$ and using Eq. (4.4):

$$\begin{aligned} \beta^{-1}[Z+1+\beta]\dot{\sigma} &= (Z+1)\left(\frac{\overline{T}-\sigma}{\varepsilon}\right)-\sigma \ , \\ -\beta^{-1}\sigma\dot{\sigma}+\dot{Z} &= -\sigma\left(\frac{\overline{T}-\sigma}{\varepsilon}\right)-Z \ . \end{aligned} \tag{4.7}$$

It follows from this formulation that the critical points satisfy the same algebraic system as does system (3.1), namely

$$\begin{aligned} &(Z+1+\varepsilon)\left(\frac{\sigma}{\overline{T}}-1\right)+\varepsilon = 0 \ , \\ &\frac{\overline{T}^2}{\varepsilon}\frac{\sigma}{\overline{T}}\left(\frac{\sigma}{\overline{T}}-1\right)-Z = 0 \ . \end{aligned} \tag{4.8}$$

Just as in Prop. 3.1, there are up to three critical points, labelled A, B, and C, for each position x in the channel.

The character of the critical points is determined by the Jacobian $\mathbf{J}$ of the right side of the system (4.3), evaluated at the critical point. Equivalently, this matrix can be calculated using Eqs. (4.5) or Eqs. (4.7), which imply that

$$\begin{aligned} &\beta^{-1}[Z+1+\beta]\,\mathbf{J} \\ &\quad = \begin{pmatrix} -\frac{1}{\varepsilon}(Z+1+\varepsilon) & -\frac{\overline{T}}{\varepsilon}\left(\frac{\sigma}{\overline{T}}-1\right) \\ \frac{\overline{T}}{\varepsilon}\left(2\frac{\sigma}{\overline{T}}-1\right)-2\beta^{-1}\sigma & -1-\beta^{-1}(2Z+1) \end{pmatrix} \qquad (4.9) \\ &\quad = \begin{pmatrix} 1 & 0 \\ \beta^{-1}\sigma & \beta^{-1}[Z+1+\beta] \end{pmatrix} \begin{pmatrix} -\frac{1}{\varepsilon}(Z+1+\varepsilon) & -\frac{\overline{T}}{\varepsilon}\left(\frac{\sigma}{\overline{T}}-1\right) \\ \frac{\overline{T}}{\varepsilon}\left(2\frac{\sigma}{\overline{T}}-1\right) & -1 \end{pmatrix} . \qquad (4.10) \end{aligned}$$

The character of the eigenvalues of J can be determined from the signs of the trace of $\mathbf{J}$, which, according to Eq. (4.9), is given by

$$-\varepsilon\beta^{-1}[Z+1+\beta]\,\mathrm{Tr}\,\mathbf{J} = Z+1+2\varepsilon+\varepsilon\beta^{-1}(2Z+1) \ ; \tag{4.11}$$

the determinant of $\mathbf{J}$, given by

$$\varepsilon\beta^{-1}[Z+1+\beta]\,\mathrm{Det}\,\mathbf{J} = Z+1+\varepsilon+\frac{\overline{T}^2}{\varepsilon}\left(2\frac{\sigma}{\overline{T}}-1\right)\left(\frac{\sigma}{\overline{T}}-1\right) \ , \tag{4.12}$$

as follows from Eq. (4.10); and the discriminant of J, given by

$$\begin{aligned}\varepsilon^2\beta^{-2}\left[Z+1+\beta\right]^2 \operatorname{Discrm} \mathbf{J} \\ = \left[Z+1-\varepsilon\beta^{-1}(2Z+1)\right]^2 - 4\overline{T}^2\left(\frac{\sigma}{\overline{T}}-1\right)\left(2[1-\varepsilon\beta^{-1}]\frac{\sigma}{\overline{T}}-1\right) .\end{aligned} \tag{4.13}$$

Because $Z > -1$ at a critical point, $\operatorname{Tr}\mathbf{J} < -2+\beta^{-1}$; thus $\operatorname{Tr}\mathbf{J} < 0$ at all critical points provided that we assume that $\beta \geq \frac{1}{2}$. Furthermore, Eq. (4.12) shows that $\operatorname{Det}\mathbf{J}$ has the same sign at the critical points as for system (3.1), *i.e.*, positive at A and C and negative at B. To determine the signs of $\operatorname{Discrm}\mathbf{J}$ at the critical points, first notice that it is positive at B because the determinant is negative. Furthermore, Eq. (4.13) defines a hyperbola similar to that defined by Eq. (3.8) and drawn in Fig. 4; it crosses the line $Z = -(1-\varepsilon\beta^{-1})/(1-2\varepsilon\beta^{-1})$ at $\sigma = \frac{1}{2}(1-\varepsilon\beta^{-1})^{-1}\overline{T}$ and $\sigma = \overline{T}$. Assuming that $\varepsilon\beta^{-1} < \frac{1}{2}$, it follows that the discriminant is positive also at A because $\sigma_B < \sigma_A < \overline{T}$ and $Z_B < Z_A < 0$. Similarly, the sign of the discriminant at C is negative unless $\overline{T}$ is near $\overline{T}_m$, just for system (3.1).

As in Prop. 3.2, these results determine the local character of orbits of the quadratic system (4.3) [and the equivalent system (4.5)] near critical points: A is an attracting node; B is a saddle point; and C is either an attracting spiral point or an attracting node. We remark that a spurt attractor C that is a node for system (3.1) might be a spiral point for system (4.3). Furthermore, Eq. (4.4) and the discussion leading to Prop. 3.4 shows that the disk bounded by the circle C_1 of radius 1 centered at $\sigma = 0$ and $Z = -1$ is positively invariant for system (4.3) (cf. Fig. 7). We assume that $\beta > 1$ so that the line $Z+1+\beta = 0$ does not cross C_1.

To rule out the existence of periodic orbits and separatrix cycles for system (4.5), the analogue of Prop. 3.3, consider the set of points Ω inside C_1 such that $\sigma < \overline{T}(1-\varepsilon\beta^{-1})^{-1}$. Because this set contains all critical points, and because it is positively invariant [because $\dot{\sigma} = -\sigma \neq 0$ along the line $\sigma = \overline{T}(1-\varepsilon\beta^{-1})^{-1}$], any periodic orbit or separatrix cycle must stay within Ω. Now introduce the scaled time variable u, defined by $du = (\overline{T}-\sigma)\,ds$, into Eq. (4.5) to obtain the equations $d\sigma/du = p(\sigma, Z)$ and $dZ/du = q(\sigma, Z)$. A straightforward calculation shows that

$$\partial p/\partial\sigma + \partial q/\partial Z = -(2\overline{T}-\sigma)/(\overline{T}-\sigma)^2 - \beta^{-1}(2Z+1)/(\overline{T}-\sigma) . \tag{4.14}$$

This quantity is strictly negative because $\sigma < 2\overline{T}$ and $Z > -2$ along an orbit in region Ω (assuming that $\varepsilon\beta^{-1} < \frac{1}{2}$). Consequently, Bendixson's criterion excludes periodic orbits and separatrix cycles for the system (4.5) and hence system (4.3).

The remaining analysis of the phase plane for the system (4.3) is almost identical to that for the system (3.1). The analysis of Sec. 3 relied on calculating the direction of flow across five curves: the circles C_1 and C_B, along which V is constant and the sign of $\dot{V}$ was determined; the circle Γ where $\dot{V} = 0$ and $\dot{\sigma}$ had a definite sign; the hyperbola where $\dot{\sigma} = 0$ and the sign of $\dot{Z}$ was known; and the parabola where $\dot{Z} = 0$. For system (4.3), V is governed by the same equation as in system (3.1). Furthermore, Eqs. (4.7) shows that $\dot{\sigma} = 0$ along the same hyperbola, and that the sign of $\dot{Z}$ on this hyperbola is the same as

before. Therefore the only difference concerns the parabola where $\Phi = \varepsilon^{-1}\sigma(\overline{T} - \sigma) - Z$ vanishes and $\dot{Z} = \beta^{-1}\sigma\dot{\sigma}$. However, $-\varepsilon\dot{\Phi} = \left[(2 + \varepsilon\beta^{-1})\sigma - \overline{T}\right]\dot{\sigma}$ when $\Phi = 0$, so that for $\sigma > \frac{1}{2}\overline{T}$ (*i.e.*, to the right of the vertex V), $\dot{\Phi}$ has the same sign as when $\beta^{-1} = 0$. Therefore the parabola works as a boundary just as in Sec. 3.

Summary: *All qualitative features of the dynamics of system (3.1) (except possibly whether C is a node or a focus) carry over to system (4.3).*

5. Qualitative Features of (JSO) Based on Phase Plane Analysis

The principal motivation of the analysis that follows is to explain recent numerical simulations of (JSO) described in Refs. [9, 11]. These exhibited several effects related to spurt: latency, shape memory, and hysteresis. Fig. 9 shows the result of simulating a "quasi-static" loading sequence in which the pressure gradient $\overline{f}$ is increased in small steps, allowing sufficient time between steps to achieve steady flow [9]. The loading sequence is followed by a similar quasi-static unloading sequence, in which the driving pressure gradient is decreased in steps. The initial step used zero initial data, and succeeding steps used the results of the previous step as initial data. The resulting hysteresis loop includes the shape memory predicted by Hunter and Slemrod [7] for a simpler model by a different approach. The width of the hysteresis loop at the bottom can be related directly to the molecular weight of the sample [9].

In this section, we explain spurt, shape memory, and hysteresis using the results of the phase plane analysis of the dynamical system (3.1) corresponding to a single relaxation time; the discussion can also be based on the system (4.3) for two relaxation times. Latency, which occurs for (JSO) when ε is sufficiently small, will be explained in Sec. 6 by means of an asymptotic analysis. The latter will also be used in Sec. 6 to show that systems (JSO) and (JSO_2) exhibit similar features when ε is sufficiently small.

We consider experiments of the following type: the flow is initially in a steady state corresponding to a forcing $\overline{f}_0$, and the forcing is suddenly changed to $\overline{f} = \overline{f}_0 + \Delta\overline{f}$. We call this process "loading" (resp. "unloading") if $\Delta\overline{f}$ has the same (resp. opposite) sign as $\overline{f}_0$. The initial flow can be described by specifying, for each channel position x, whether the flow is at a classical attractor A (x is a "classical point") or a spurt attractor C (x is a "spurt point") for the system (3.1) with $\overline{T} = -\overline{f}_0 x$. We shall say that any point lying on the same side of the stable manifold of B as is A lies on the "classical side"; points lying on the other side are said to be on the "spurt side." The outcome of the experiment depends on the character of the phase portrait with $\overline{T} = -\overline{f}x$. To determine this outcome, we need only decide when a classical point becomes a spurt point or *vice versa*.

To understand how critical points move, consider Fig. 10. First notice that the critical points for Eq. (3.1), for any value of $\overline{T}$, lie on the circle Γ, which is independent of $\overline{T}$. Let $M = (\sigma_M, Z_M)$ denote the degenerate (double root) critical point that occurs when $\overline{T} = \overline{T}_M$, *i.e.*, at "top jumping" in Fig. 2; and let $m = (\sigma_m, Z_m)$ denote the degenerate critical point for $\overline{T} = \overline{T}_m$, *i.e.*, for "bottom jumping." These points, together with their reflections $M' = (-\sigma_M, Z_M)$ and $m' = (-\sigma_m, Z_m)$, serve to divide Γ into arcs: Γ_A, the upper arc of Γ between M and M'; Γ_C, the lower arc between m and m'; and Γ_B, the remaining two arcs where $Z \in [Z_m, Z_M]$. For any value of $\overline{T}$, positive or negative, the

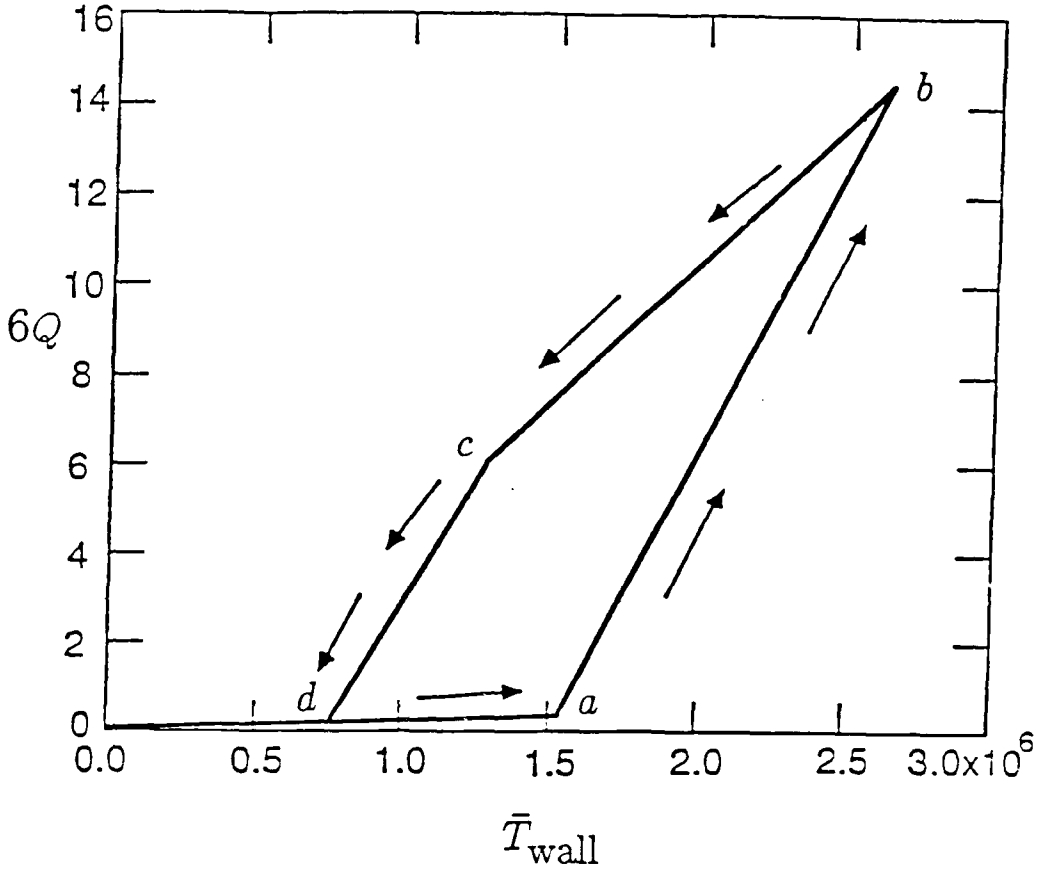

Fig. 9: Hysteresis under cyclic load: normalized throughput $6Q$ *vs.* wall shear stress $\overline{T}_{\text{wall}}$ [9].

classical attractor A lies in Γ_A, the spurt attractor C lies in Γ_C, and the saddle point B lies in Γ_B. Furthermore, as $|\overline{T}|$ is increased, the critical points A and C move downward along Γ, while B moves upward. This follows from Eq. (3.3) by differentiating the relation $Q(\sigma/\overline{T}) = 0$, which determines how $\sigma/\overline{T}$ varies with $\overline{T}$, and by using the first of Eqs. (3.2).

The principle mathematical properties of the dynamical system (3.1) that determine the outcome of loading and unloading experiments are embodied in

Proposition 5.1:

(1) A classical point A_0 for the initial forcing $\overline{f}_0$ lies in the domain of attraction of the classical attractor A for $\overline{f}$, provided that A exists (i.e., $|\overline{f}x| < \overline{T}_M$);

(2) A spurt point C_0 for the initial forcing $\overline{f}_0$ lies in the domain of attraction of the spurt attractor C for $\overline{f}$ unless (a) C does not exist (i.e., $|\overline{f}x| < \overline{T}_m$); or (b) C lies on the classical side of the stable manifold of the saddle point B for $\overline{f}$.

This follows because, as shown in Secs. 3 and 4 (see Prop. 3.5), the stable manifold of B, which separates the domain of attraction of A from that of C, never crosses the arc Γ_A. We remark that (2b) occurs only when $|\Delta\overline{f}|$ is large enough. In particular, it never occurs during a quasi-static processes, in which the flow is allowed to attain equilibrium

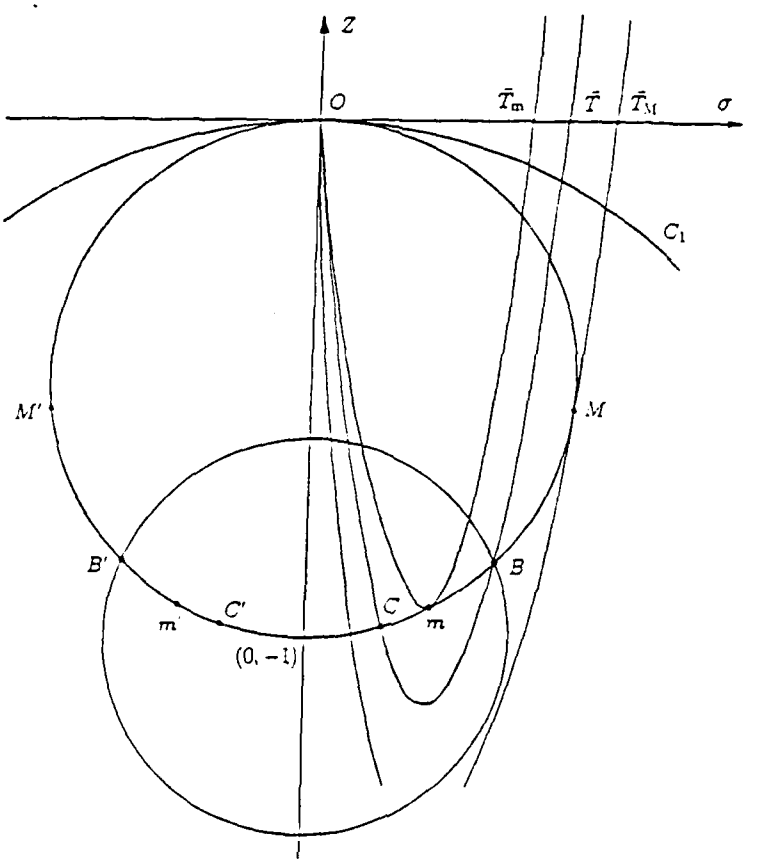

Fig. 10: Location of critical points.

after each of many small increments in forcing.

A. Startup

As a first experiment, consider starting with $\overline{f}_0 = 0$ and loading to $\overline{f} > 0$. Thus the initial state for each x lies at the origin $\sigma = 0$, $Z = 0$. Then according to 5.1(1) above, each $x \in [-1/2, 0]$ such that $\overline{f}|x| < \overline{T}_M$ is a classical point, while the x for which $\overline{f}|x| > \overline{T}_M$ are spurt points (because there is no classical attractor). Consequently, we draw two conclusions:

Proposition 5.2:

(a) *If the forcing is subcritical (i.e., $\overline{f} < \overline{f}_{\text{crit}} := 2\overline{T}_M$), the asymptotic steady flow is entirely classical.*

(b) *If the forcing is supercritical ($\overline{f} > \overline{f}_{\text{crit}}$), there is a single kink in the velocity profile (see Fig. 3), located at $x_* = -\overline{T}_M/\overline{f}$; those $x \in [-1/2, x_*)$, near the wall, are spurt points, whereas $x \in (x_*, 0]$, near the centerline, are classical.*

The solution in case (b) can be described as "top jumping" because the stress $\overline{T}_* = \overline{T}_M$ at the kink is as large as possible, and the the kink is located as close as possible to the wall.

B. Loading

Next, consider increasing the load from $\overline{f}_0 > 0$ to $\overline{f} > \overline{f}_0$. A point x that is classical for $\overline{f}_0$ remains classical for $\overline{f}$ unless there is no classical attractor for $\overline{T} = -\overline{f}x$, *i.e.*, $\overline{f}|x| > \overline{T}_M$. A spurt point x for $\overline{f}_0$, on the other hand, is always a spurt point for $\overline{f}$. This is true because: (a) the spurt attractor always exists at the larger total stress $\overline{T} = -\overline{f}x$; and (b) the stable manifold of B does not cross the arc of Γ between C and B, and C_0 lies on this arc, so that C_0 lies on the spurt side of the stable manifold of B.

As a result, a point in x in the channel can change only from a classical attractor to a spurt attractor, and then only if $\overline{f}|x|$ exceeds $\overline{T}_M$. When $\overline{f}$ is chosen to be supercritical, loading causes the position x_* of the kink in Fig. 3 to move away from the wall, but only to the extent that it must: a single jump in strain rate occurs at $x_* = -\overline{T}_M/\overline{f}$, where the total stress is $\overline{T}_* = \overline{T}_M$. These conclusions are valid, in particular, for a quasi-static process of gradually increasing the load from $\overline{f}_0 = 0$ to $\overline{f} > \overline{f}_{\text{crit}}$.

C. Unloading

Now consider unloading from $\overline{f}_0 > 0$ to $\overline{f} < \overline{f}_0$; assume, for the moment, that $\overline{f}$ is positive. Here, the initial steady solution need not correspond to top jumping. For this type of unloading, a point x that is classical for $\overline{f}_0$ always remains classical for $\overline{f}$: the classical attractor for $\overline{f}$ exists because $\overline{f}|x| < \overline{f}_0|x|$. By contrast, a spurt point x for $\overline{f}_0$ can become classical at $\overline{f}$. This occurs if: (a) the total stress $\overline{T} = -\overline{f}x$ falls below $\overline{T}_m$; or (b) the spurt attractor C_0 for $\overline{T} = -\overline{f}_0 x$ lies on the classical side of the stable manifold of the saddle point B for $\overline{T} = -\overline{f}x$ [see Prop. 5.1(2b)]. The latter possibility can cause the formation of a second kink in the steady velocity profile, which arises from a second jump in the plot of steady shear stress *vs.* strain rate shown in Fig. 11. A new region of classical flow develops next to the wall, and the internal region of spurt flow lies between the two classical regions. Of course, this occurs only if $|\Delta f| = |\overline{f} - \overline{f}_0|$ is sufficiently large, i.e., the unloading is abrupt. However, it is impossible to have classical flow regions to start spurting, even under sudden finite loading, unless the classical attractor disappears. In a quasi-static experiment, in which the forcing is decreased gradually, spurt points can become classical only if $\overline{f}|x| < \overline{T}_m$.

D. Quasi-Static Loading and Unloading: Shape Memory and Hysteresis

We now discuss the quasi-static loading-unloading cycle, illustrated in Fig. 9, based on results of Subsections B. and C. Specifically, recall that there are two ways in which a spurt point x can become classical during unloading: (i) if $\overline{T}_*$ decreases to $\overline{T}_m$, or (ii) if case (b) in Subsection C occurs. For a fixed ϵ, the latter can be avoided in quasi-static unloading by keeping the increments $|\Delta|$ sufficiently small.

Consider a quasi-static loading-unloading cycle that starts with zero forcing, loads to a $\overline{f}_{\text{max}} > \overline{f}_{\text{crit}}$, and then unloads to $\overline{f}_{\text{final}} < \overline{f}_{\text{crit}}$; of course, $\overline{f}_{\text{final}}$ may be zero. At first, while $\overline{f} < \overline{f}_{\text{crit}}$, the flow is classical (from the origin to a in Fig. 9). When $\overline{f}$ becomes supercritical (from a to b in Fig. 9), a kink forms at the wall; the total stress at the kink is $\overline{T}_* = \overline{T}_M$, and the position x_* moves out from the wall according to the rule $x_* = -\overline{T}_M/\overline{f}$. The thickest spurt layer occurs at $\overline{f}_{\text{max}}$ (b in Fig. 9), for which $x_* = x_{\text{max}} = -\overline{T}_M/\overline{f}_{\text{max}}$. Upon unloading (from b to c to d in Fig. 9), the layer position x_* remains fixed at x_{max}, and the stress is $\overline{T}_* = (\overline{f}/\overline{f}_{\text{max}})\overline{T}_M$, so long as $\overline{T}_*$ remains above $\overline{T}_m$; this occurs between b and c in Fig. 9 and corresponds to shape memory, in the sense that the layer position

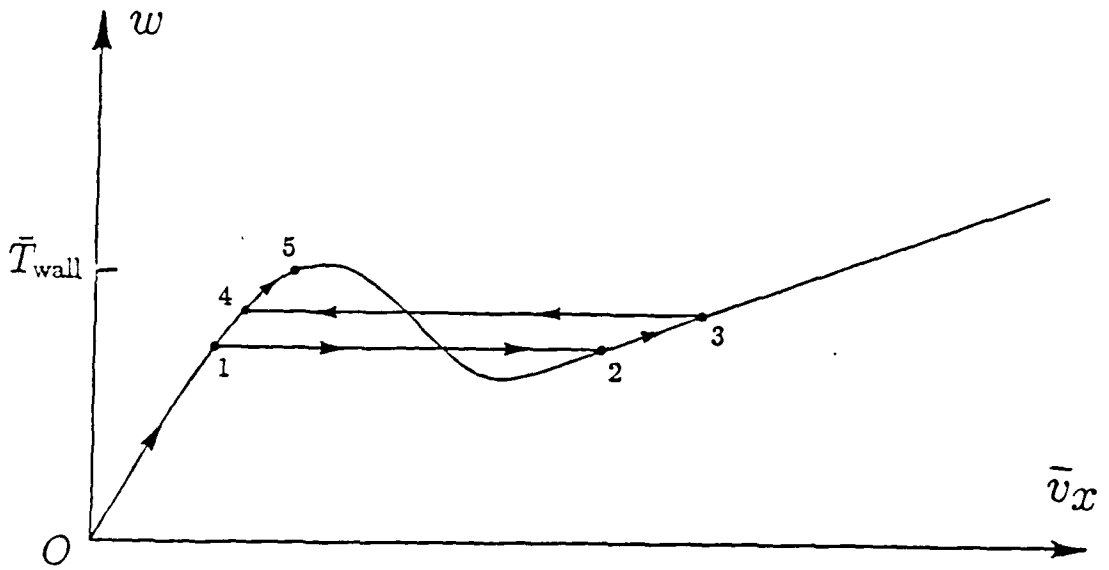

Fig. 11: Generation of flow with two kinks, giving rise to an internal spurt layer. The sequence of relevant strain rates, $\overline{v}_x$, labeled 1 – 5, is shown as the stress, w, varies linearly across the channel.

remains fixed, and points on the interval $[-1/2, x_*)$ remain spurt points, while points on the interval $(x_*, 0]$ remain classical. Notice that this behavior gives rise to hysteresis, in the sense that no part of the loading curve in Fig. 9 is retraced until the entire flow becomes subcritical. If $\overline{f}_{\text{final}}$ is small enough, then eventually $\overline{T}_*$ falls below $\overline{T}_m$, whereupon the layer position x_* moves toward the wall: $x_* = -\overline{T}_m/\overline{f}$, and the stress at the kink is $\overline{T}_m$; this occurs between c and d in Fig. 9 and corresponds to loss of shape memory. If x_* reaches the wall (at d in Fig. 9), then the flow becomes entirely classical.

Summary: *A kink moves away from the wall under loading if it is a top jumper; it moves toward the wall under unloading if it is a bottom jumper; and otherwise it remains fixed. The hysteresis loop opens from the point at which unloading commences; no part of the unloading path retraces the loading path until point d of Fig. 9 is reached.*

E. Reloading and Flow Reversal

It is possible, of course, to apply more complex loading and unloading sequences than those described in Subsection D. For example, a loading sequence can be followed by unloading, which, in turn, is followed by reloading. Arguments extending the ones given above can be used to make qualitative predictions in such cases. In particular, Prop. 5.1 implies that the layer position can remain fixed upon reloading (*i.e.*, shape memory is retained).

Next we consider flow reversals, which occur when $\overline{f}_0$ and $\overline{f}$ have opposite signs. In flow reversal with loading, *i.e.*, $|\overline{f}| \geq |\overline{f}_0|$, a mild generalization of the argument of Subsection B. that the kink position x_* moves away from the wall, and all conclusions hold with appropriate change in sign. To see this, it is helpful to examine Fig. 10 with appropriate parabolas and circles Γ and C_B constructed also in the left half-plane; this will also be useful in what follows. A striking phenomenon has been observed in numerical experiments using data in Ref. [17], in the case flow reversal in which a spurted solution is unloaded, *i.e.*, $\overline{f}_0$ and $\overline{f}$ have opposite signs and $|\overline{f}| \leq |\overline{f}_0|$. Surprisingly, numerical experiments indicate that in such a process the layer position can remain unchanged, and shape memory can be retained. For this to happen, the magnitude of the stress at the layer boundary must not fall below $\overline{T}_m$. Given this fact, there is a variety of phase portraits constructed with the aid of Fig. 10 that can lead to retention of shape memory in flow reversal with unloading. Perhaps the simplest way this can occur is to load continuously to a supercritical load level $\overline{f}_0 > 0$ to obtain a top-jumping solution of the system (3.1) in which all spurt points $x \in [-1/2, x_*)$ have only a single critical point C_0. Reversing this flow with unloading, leads to solutions in which all points $x \in (x_*, 0]$ remain classical; observe that circles C_B in Fig. 10 are symmetric about the Z-axis, and by symmetry, Prop. 5.1(1) implies the result. It is clear that points $x \in [-1/2, x_*)$ for which $\overline{T} \geq \overline{T}_M$ will remain spurt points. The only remaining issue concerns points $x \in [-1/2, x_*)$ for which $\overline{T}_m \leq \overline{T} \leq \overline{T}_M$. For these to remain spurt points, the stable manifold of B must extend far enough into the right half-plane to enclose the spurt attractors C_0. General criteria for this situation to occur are not so easy to establish; however, it will be seen in Sec. 6 that for ε as small as in Ref. [17], this situation is likely to occur. By contrast, there are many ways to lose shape memory particularly if ε is not small.

6. Asymptotic Analysis of (JSO) and (JSO_2) for $\alpha = 0$ and Small ε

The analysis of system (JSO) leads to analytical description that accurately reflects the experimental results of Vinogradov *et al.* [17]. It raises a question of the physical interpretation of the Newtonian viscosity. This was chosen to give the total stress *vs.* strain rate curve local extrema and evidently led to an empirical model with mathematical features that reproduce observed behavior. To make the predictions of this model credible, the empirical parameter ε must be associated with a measurable physical quantity. Since there is no solvent associated with the undiluted systems studied by Vinogradov *et al.*, the most likely interpretation of the Newtonian contribution is that is somehow represents the effects of shorter relaxation times. At first sight this seems puzzling in that the full system (2.9) is not classifiable according to type when $\eta \neq 0$ but is hyperbolic (away from the elliptic region) when $\eta = 0$; a small amount of Newtonian viscosity seems to make a large difference in the mathematical character of system (2.9). In Sec. 4, we saw that in the region of parameter space characteristic of the data of Vinogradov *et al.*, system (JSO) and system (JSO_2) exhibit the same steady behavior and very similar dynamic behavior. This suggests that it may be valid to approximate system (JSO_2) by the simpler system (JSO). In this section, we show that the dynamic behavior of subcritical solutions and of critical solutions during the latency phase in the two models agrees to $O(\varepsilon^2)$. Since the existence, location, and nature of the critical points of system (JSO) and system (JSO_2) is identical (for $\beta \geq 1$) and the phase portraits are qualitatively the same, the only possible difference between the two models can be seen to lie in the precise timing of the "Newtonian phase" [11] and the details of the spurt transition following latency.

The following calculations involve system (JSO_2) but are valid for system (JSO) in the limit as $\beta \to \infty$. A major point is that many of the results are independent of β. We consider the case when $\varepsilon \ll 1$; this is true for the data of Vinogradov *et al.*that exhibit spurt, where ε is in the range $O(10^{-2})$ to $O(10^{-3})$. Equation (4.4) shows that solutions of system (JSO_2), with initial data at the origin, on time scales of order ε, very nearly follow the arcs of circles defined by the right side of the equation. Equation (4.5) shows that such solutions will change on an $O(\varepsilon)$ time scale until $\sigma = \overline{T} - O(\varepsilon)$. The time during which this occurs is referred to as the "Newtonian phase." In principle, it is possible to obtain higher order estimates, but for our purposes, it will be sufficient to omit terms of order ε and higher and approximate the value of Z at the end of the Newtonian phase by that value on the circle corresponding to $\sigma = \overline{T}$. This value is

$$Z_N = \sqrt{1 - \overline{T}^2} - 1 \tag{6.1}$$

There are two important points to be made here. First, for $T > 1$ spurt starts immediately and there is no Newtonian or latent phase. Second, the behavior of systems (JSO) and (JSO_2) differs only by a factor of $\beta^{-1}(Z + 1 + \beta)$ in the time scale and, to $O(\varepsilon)$, they have the same orbits during the Newtonian phase. We now consider system (JSO_2) during the latent phase, which begins when Eq. (6.1) holds approximately.

We make a formal asymptotic expansion of the solution (σ, Z) of the system (4.6) in powers of ε,

$$\begin{aligned} \sigma &= \sigma_0 + \varepsilon\sigma_1 + \varepsilon^2\sigma_2 + \dots \\ Z &= Z_0 + \varepsilon Z_1 + \varepsilon^2 Z_2 + \dots \end{aligned} \tag{6.2}$$

Multiplication of Eqs. (4.7) by ε and substitution of Eqs. (6.2) readily yields the following result upon comparing terms through first order in ε:

$$\begin{aligned} \sigma_0 &= \overline{T} \\ \sigma_1 &= -\frac{\overline{T}}{Z_0+1} \\ \dot{Z}_0 &= -\frac{\overline{T}^2}{Z_0+1} - Z_0\,; \end{aligned} \tag{6.3}$$

Z_N provides an initial value for Z_0 in the solution of the third equation for Z_0. Thus σ stays nearly constant while Z varies at zero order. This is a key point: The long relaxation mode response of the system is a rapid development of σ. At early time, during latency, σ balances the pressure gradient by assuming the linear profile of $\overline{T}$. During this time, the normal stresses, which are self-equilibrating in that they play no direct role in balancing the pressure gradient, grow on a very different time scale. The solution of the third equation of (6.3), which we call the "latency equation" is independent of all parameters of the model except $\overline{T}$. For $1/2 < \overline{T} < 1$, latency ends when Z_0 is sufficiently close to -1; for this value of Z_0, σ_1 becomes singular, and spurt ensues. For $\overline{T} < 1/2$, as we have seen from the phase plane analysis, orbits starting at the origin do not move to the spurt attractor. The latency time can be easily found by solving for the inverse function in the third equation of (6.3), which can be done analytically; the duration of the Newtonian phase can be neglected, and the integration can be performed from $Z_0 = Z_N$ to $Z_0 = -1$, as follows

$$\begin{aligned} t_{\text{latency}} = \int_{Z_N}^{-1} \frac{Z+1}{Z^2+Z+\overline{T}}\,dZ &= \tfrac{1}{2}\ln\left(\frac{\overline{T}^2}{Z_N^2+Z_N+\overline{T}^2}\right) \\ &+ \frac{1}{\sqrt{4\overline{T}^2-1}}\tan^{-1}\left(\frac{-1}{\sqrt{4\overline{T}^2-1}}\right) - \frac{1}{\sqrt{4\overline{T}^2-1}}\tan^{-1}\left(\frac{2Z_N+1}{\sqrt{4\overline{T}^2-1}}\right) \end{aligned} \tag{6.4}$$

The resulting latency time is non-dimensional and thus scales with λ^{-1} for a fixed $\overline{T}$. The non-dimensional latency time decreases with increasing $\overline{T}$, because the initial value given by Eq. (6.3) gets closer to one and the integrand of Eq. (6.4) decreases. For $\overline{T} < 1/2$, one finds that the integral with the given limits does not exist, so that in this sense, the latency time of a classical solution is infinite. Note that these results for system (JSO_2) are independent of β, and thus apply equally to system (JSO).

Numerical initial values for the coefficients of Eqs. (6.2) at the first two orders can be determined from matched asymptotic expansions in the spirit of Ref. [10]. It turns out that all expansion terms through order one, except Z_1, of an inner expansion with time stretched by $t_* := t/\varepsilon$ have finite asymptotic values as $t_* \to \infty$. A value of Z_1 can be obtained by taking the value obtained when the coefficients of zero order are within $O(\varepsilon^2)$ of their asymptotic values, and the coefficients of first order are within $O(\varepsilon)$ of their asymptotic values. This procedure yields initial data for the outer expansion, Eq. (6.2) from the inner expansion; it is not sensitive to the precise values of the "O-constants" involved.

Continuing the outer expansion at second order, we find that σ_2 and Z_1 satisfy

$$\begin{aligned} \beta^{-1}(Z+1)\dot{\sigma}_1 + \dot{\sigma}_1 &= -(Z_0+1)\sigma_2 - (Z_1+1)\sigma_1 \\ -\beta^{-1}\sigma_0\dot{\sigma}_1 + \dot{Z}_1 &= \sigma_0\sigma_2 + \sigma_1^2 - Z_1 \end{aligned} \tag{6.5}$$

Since σ_1 is known, the first equation reduces to an algebraic equation for σ_2 in terms of known quantities and Z_1; substitution into the second equation gives an ordinary differential equation, with known coefficients, for Z_1. There is an interesting feature of such a solution. Multiplying the first equation by σ_0 and the second by Z_0+1 and adding yields

$$(Z_0+1)\dot{Z}_1 + \sigma_0\dot{\sigma}_1 = (Z_0+1)\sigma_1^2 - (Z_0+1)Z_1 + \sigma_0(Z_1+1)\sigma_1 \tag{6.6}$$

So Z_1 is determined by an ODE whose coefficients are independent of β, and if initial data is given for Z_1 that is independent of β, then

$$\begin{aligned} \sigma_2 &= f_1(\beta, \overline{T}, Z_0, Z_1) \\ \dot{Z}_1 &= f_2(\overline{T}, Z_0, Z_1) \end{aligned} \tag{6.7}$$

Thus systems (JSO_2) and (JSO) agree to two orders in ε in their behavior during the latent phase, when their initial data agree to that level of accuracy. However, the value of Z_1 obtained from the matching procedure described above, and the precise value t_* at which the matching criteria are met are functions of β. This leads to the conclusion that the two systems (JSO_2) and (JSO) agree to order $O(\varepsilon)$ in the Newtonian phase; during the latency phase, the difference between the models accumulates further only at order $O(\varepsilon^2)$. Moreover, changing the values of the O-constants in matching does not alter this conclusion.

By a perturbation analysis of the roots of system (2.22) for small ε, one finds that at the spurt attractor

$$\begin{aligned} \sigma &= \frac{\varepsilon}{\overline{T}}\left[1 + \frac{\varepsilon}{\overline{T}^2} + O(\varepsilon^2)\right] \\ Z &= -\left[1 + O(\varepsilon^2)\right] \end{aligned} \tag{6.8}$$

An important consequence of (6.8) relates to retention of shape memory in flow reversal. Note that the distance from C_0 to C is of order ε, and recall from Sec. 5E that shape memory is lost only if the stable manifold of B separates C_0 and C.

Continuing the asymptotic analysis of spurt dynamics, inspection of Eqs. (3.1) or (4.3) indicates that in the early stages of spurt, when Z is not near -1 and σ has deviated from $\overline{T}$ after latency, the derivatives of the system are $O(\varepsilon^{-1})$. A stretched-time series like that for the Newtonian phase would be appropriate; analysis of the Newtonian phase then suggests that the two systems could differ in their spurt dynamics at least at first order, but of course, they would end up in the same steady states. The conclusion is that systems (JSO_2) and (JSO) have the same critical points and qualitatively similar orbits. In the asymptotic range studied here, they have virtually identical latency times.

The remaining task is to study possible differences between (JSO) and (JSO_2) that may occur during the spurt phase, and predict dynamic behavior that may be observable

in experiments. The analysis that follows will determine the detailed structure of orbits spiraling into the spurt attractor C, for example in Fig. 7, in as large a neighborhood of C as permitted. One objective is to determine the frequency at which orbits spiral toward C. We use the scaled system (4.5) that approximates JSO_2. Define $X := (\sigma, Z)^T$ and write $X = X_0 + \tilde{X}$, where $X_0 = (\sigma_0, Z_0)^T$ is a critical point. Then the rescaled system (4.5) is of the form $X' = F(X)$; by Taylor's theorem, the latter can be written as

$$\tilde{X}' = \mathbf{J}\tilde{X} + \frac{1}{2}\tilde{X}^T D^2 F(X_0)\tilde{X} \ , \tag{6.9}$$

where D denotes differentiation with respect to X, $F(X_0) = 0$, $DF(X_0) = \mathbf{J}$ of Eq. (4.9), and D^2F is the Hessian. The Taylor series stops at second order because the system is quadratic. We convert system (6.9) to polar coordinates in the phase plane, with origin at X_0, by defining r and θ implicitly:

$$\begin{aligned} \sigma &= \sigma_0 + r\cos\theta \\ Z &= Z_0 + r\sin\theta \ , \end{aligned} \tag{6.10}$$

and we obtain

$$(\ln r)' = \frac{\tilde{\sigma}\tilde{\sigma}' + \tilde{Z}\tilde{Z}'}{r^2} \tag{6.11}$$

$$\theta' = \frac{\tilde{\sigma}'\tilde{Z} - \tilde{\sigma}\tilde{Z}'}{r^2} \ . \tag{6.12}$$

We shall evaluate these derivatives centered at the spurt attractor, C, when it is a spiral point. The ratio of these two derivatives, $d\ln r/d\theta$, when the numerator is negative, is the rate of motion toward the attractor compared with the angular frequency of spiraling around the attractor.

Applying Eqs. (6.9) and 6.10 leads directly to

$$\tilde{X}' = \mathbf{J}\tilde{X} + \begin{pmatrix} -\varepsilon^{-1}\tilde{\sigma}\tilde{Z} \\ \varepsilon^{-1}\tilde{\sigma}^2 - \beta^{-1}r^2 \end{pmatrix} \ . \tag{6.13}$$

Note that it is much easier to determine the quadratic terms from direct inspection of system (4.5), rather than formal evaluation of the second derivative in Eq. (6.9). It is a simple matter to use Eq. (6.13) to derive a general expression for $d\ln r/d\theta$, but the expression is rather complicated; it is greatly simplified when evaluated at C, using the asymptotic formulas Eqs. (6.8) to evaluate σ_0, Z_0. Rescaling back to real time, the result is

$$\frac{d\ln r}{d\theta} = \frac{\varepsilon\left(-1 + \frac{\tilde{\sigma}\tilde{Z}}{r^2 T} - \beta^{-1}\left[\tilde{Z} - \frac{\tilde{Z}}{r^2}^2\right]\right)}{\overline{T} - \tilde{\sigma} - \varepsilon\left(\frac{1}{T}\left(1 - \frac{\tilde{\sigma}^2}{r^2}\right) + \beta^{-1}\left[\tilde{\sigma} - \frac{\tilde{\sigma}\tilde{Z}}{r^2}\right]\right)} + O(\varepsilon^2) \ . \tag{6.14}$$

There are several restrictions on the use of Eq. (6.14) contained in the inequalities that follow. These are asymptotically valid to order $O(\varepsilon)$; that is they may require the addition

of a term of magnitude at most order $O(\varepsilon)$ to make them true. The first restriction is that the change in the time scale (see Eq. (4.5)) be valid (*i.e.*, that the denominators in Eq. (4.3) do not vanish). This is assured by requiring

$$\beta^{-1}\tilde{Z} > -1 \,. \tag{6.15}$$

Also r and $\overline{T}$ must be restricted so that the solution spirals into the spurt attractor, C, e. g., by requiring the numerator on the right side of Eq. (6.13) to be negative, while the denominator is positive. This yields the following asymptotic inequalities that are sufficient to produce spiraling:

$$\begin{aligned} &0 < r < r_0 \leq \min\{\beta - 1, \overline{T}\} \\ &\overline{T} \geq \frac{1}{2 - 2\beta^{-1}(r_0 + 1)} \,. \end{aligned} \tag{6.16}$$

These inequalities may be applied by restricting r_0 on the basis of $\beta - 1$ alone and applying the second inequality in Eq. (6.16) to determine $\overline{T}$; if necessary, r_0 can then be further restricted to satisfy the first of inequalities (6.16). Note that $\overline{T}$ can never be smaller than $1/2$, so that C is always a spiral point. Spiral orbits are observed for $\overline{T}$ smaller than $1/2$, but restrictions on r that are more optimal than made in (6.16) would be required in such cases. We emphasize that the restrictions imposed on r are much less severe than would be implied by retaining only linear terms in Eq. (6.9).

The key observation for determining the frequency of spiraling toward C is that both linear and nonlinear terms of order ε^{-1} cancel in the radial equation, Eq. (6.11), and thus in the numerator of Eq. (6.14); this can be seen from Eqs. (4.9) and (6.13) (note there are both linear and nonlinear contributions to the angular frequency of order ε^{-1}). Thus the orbits are elliptical spirals with decay rates of order $O(\varepsilon)$ in the radial component; as $\varepsilon \to 0$, the orbits tend to circles. These conclusions hold as far from C as permitted by the inequalities of Eq. (6.16). We can also see that for $\beta > 1$, the effect of β is to modify the decay rate of the radial component to relative order $O(1)$, but the effect is only at relative order $O(\varepsilon)$ in angular frequency. For small values of ε, the decay rate is sufficiently small that the behavior could be mistaken for undamped oscillation of the stresses.

7. Physical Implications

The results of Sec. 5 provide an explanation of the spurt phenomenon in the context of a model that is analyzed in sufficient detail to identify a number of new features that should experimentally observable. We will summarize these predictions below. First, it is important to note that there is a conclusion of our analysis that on the accuracy of these predictions: When momentum transfer is not important in the dynamic process (that is, when it is a valid approximation to set α to zero in (JSO) and (JSO_2), a small amount of Newtonian viscosity in system (JSO) accurately mimicks the behavior of system (JSO_2) with $\delta = 0$ and small ε. This is true in spite of the fact that (JSO_2) is hyperbolic while (JSO) cannot be classified according to type. We expect that this observation extends to other models and provides some quantitative reinforcement to the belief among rheologists that Newtonian viscosity can be a useful modeling tool in undiluted systems.

One of the widely accepted explanations of spurt and similar observations is that the presence of the wall affects the dynamics of the polymer system near the wall. Conceivably, there could be a variety of "wall effects," the most obvious is the loss of chemical bond between wall and fluid, or wall slip [5]. Perhaps the most distinguishing feature of our alternative approach is: it predicts that spurt stems from a material property of the polymer and is not related to any external interaction. The spurt layer forms at the wall in situations such as top jumping because the stresses are higher there; for the same reason, of course, is chemical bonds would break at the wall;however, our approach predicts that the layer of spurt points spreads into the interior of the channel on continued loading. Layer thickness is predicted to grow continuously in loading to a thickness that should be observable, provided secondary (two-dimensional) instabilities do not develop.

Our analysis suggests other ways in which experiments might be devised to verify the dependence of spurt on material properties: (i) produce multiple kinks with spurt layer separated from the wall, (ii) produce hysteresis in flow reversal (Fig. 9). Our model predicts circumstances under which a different path can be followed in sudden reversal of the flow than would be followed by a sequence of solutions in which the pressure gradient is reduced to zero and reloaded again (with the opposite sign) to a value of somewhat smaller magnitude. Such behavior does not seem likely to be explainable by a wall effect.

An observation that has been associated with spurt and related phenomena is the variation in kinematic quantities that appears to be periodic; such variations are inferred from the appearance of extrudates at the exit of a die or capillary in which spurt (or slip, or other wall effect) is presumed to be occurring. The analysis in Sec. 6 does not predict any truly periodic behavior, but the spiraling into the spurt attractor is shown to have a very high frequency and slow decay rate, so that for practical polymer systems, it may very well appear to be periodic and persistent. Furthermore, since these oscillations involve large changes in the normal stresses, they could very well lead to "periodic distortions" in the stream extruded from a die in which such behavior is occurring. Our prediction is that the average "period" of such distortions would be proportional to the viscosity ratio, ε; however, because of the $-\tilde{\sigma}/\varepsilon$ term in the denominator of Eq. (6.14), the apparent period could vary significantly in time until the magnitude of the $\tilde{\sigma}$ contribution to the shear stress is small compared to ε. The "ultimate period" is predicted to be inversely proportional to $\overline{T}$, to leading order.

Even if it can be established that spurt is a distinct phenomenon from wall slip (or other wall effects), our model is not the only possible alternative. Others have proposed that spurt is related to non-monotone constitutive behavior (see for example Refs. [6], [15], or [12]). The features of hysteresis deduced in Sec. 5D stand in marked contrast to other plausible predictions of the nature of the hysteresis in spurt [12]; experiments could be devised to verify which theory is correct.

Finally, the most important and perhaps the easiest experiment to perform to verify our theory is to produce latency. Eq. (6.4) predicts long latency times for data corresponding to realistic material data; no sophisticated timing device would be required, nor would the onset of the instability be hard to identify. The increase in throughput is predicted to be so dramatic that simple visual inspection of the exit flow would probably be sufficient.

8. Conclusions

Phase-plane and small parameter asymptotic techniques have been used to analyze single and two relaxation-time models that approximate the behavior of highly elastic polymeric liquids in shear flow through slit dies driven by a pressure gradient. Results of the analysis show that both models exhibit the same qualitative features for realistic data based on polymer melts. The results provide an explanation of the spurt phenomenon observed experimentally; this explanation differs from "wall slip" in that it stems solely from material properties of the polymer and not from the interaction of the polymer with the walls. In addition, the analysis predicts new phenomena that should be observable in new experiments: latency, shape memory, and hysteresis in cyclic loading and loading that induces sudden flow reversals. The key to understanding the dynamics of the approximating systems is fixing the location of the discontinuity in the strain rate induced by the non-monotone character of the steady shear stress *vs.* strain rate.

Although our analysis applies only to the special constitutive models we have studied, we expect that the qualitative features of our results appear in a broad class of non-Newtonian fluids. Our analysis has identified certain universal mathematical features in the shear flow of viscoelastic fluids described by differential constitutive relations that give rise to spurt and related phenomena. Since we have seen that the qualitative features of two models, (JSO), and (JSO_2) are very similar in the range of interest, we choose to describe the universal features by abstracting (JSO). The key feature is that there are three widely separated time scales, each associated with an important non-dimensional number (α, ε, and 1, respectively), when scaled by the dominant relaxation time, λ^{-1}. Each of these time scales can be associated with a particular equation in system (JSO):

$$\begin{aligned} \tau_{\mathbf{parab}} &:= \rho h^2 \lambda/\mu & \alpha &= \tau_{\mathbf{parab}}\lambda \\ \tau_{\mathbf{shear}} &:= \eta/\mu & \varepsilon &= \tau_{\mathbf{shear}}\lambda \\ \tau_{\mathbf{normal}} &:= \lambda^{-1} & 1 &= \tau_{\mathbf{normal}} \,. \end{aligned} \tag{8.1}$$

Note that $\tau_{\mathbf{shear}}$ can be associated with with μ_2/λ_2, a secondary shear viscosity in system (JSO_2). We assume that $\tau_{\mathbf{parab}} \ll \tau_{\mathbf{shear}} \ll \tau_{\mathbf{normal}}$, as in experiments of Vinogradov *et al.* [17].

To see how these time scales are associated with specific equations, it is convenient to

rewrite system (JSO)in the following equivalent form:

$$\begin{aligned}
&\alpha v_t - \sigma_x = \varepsilon v_{xx} + f \\
&\sigma_t - (Z+1)\,\frac{\bar{T} + \alpha \int_0^x v_t(x',t)dx'}{\varepsilon} = -\left[\frac{(Z+1)}{\varepsilon} + 1\right]\sigma \\
&Z_t + \sigma\frac{\bar{T} - \sigma + \alpha \int_0^x v_t(x',t)dx'}{\varepsilon} = -Z\ .
\end{aligned} \tag{8.2}$$

Setting $\alpha = 0$ in system (8.2) yields the approximating system (3.1): the extreme smallness of τ_{parab} allows us to disregard inertial effects of the first equation. So long as $Z+1$ is not $O(\varepsilon)$, therefore, the effective relaxation time in the second equation is ε. Consequently, σ achieves its steady or latent value on a time scale of order τ_{shear}. Finally, as a consequence of the third equation, Z tends either to a classical steady state value (less than $-1/2$), or, in case of spurt, to a value near -1 with effective relaxation time 1. We conclude that it is this general structure of evolution equations governing the flow that causes the approach to spurt to have three distinct phases.

Acknowledgments

We thank Professor A. Coppel for suggesting an elegant argument that rules out the existence of periodic and separatrix cycles for the systems (3.1) and (4.3). We also acknowledge helpful discussions with D. Aronson, M. Denn, G. Sell, M. Slemrod, A. Tzavaras, and M. Yao.

References

1. A. Andronov and C. Chaikin, *Theory of Oscillations*, Princeton Univ. Press, Princeton, 1949.

2. R. Bird, R. Armstrong, and O. Hassager, *Dynamics of Polymeric Liquids*, John Wiley and Sons, New York, 1987.

3. E. Coddington and N. Levinson, *Theory of Ordinary Differential Equations*, McGraw-Hill, New York, 1955.

4. A. Coppel, private communication, 1989.

5. M. Denn, "Issues in Viscoelastic Fluid Dynamics," *Ann. Rev. Fluid Mech.*, 1989. To appear.

6. M. Doi and S. Edwards, "Dynamics of Concentrated Polymer Systems," *J. Chem. Soc. Faraday* **74** (1978), pp. 1789–1832.

7. J. Hunter and M. Slemrod, "Viscoelastic Fluid Flow Exhibiting Hysteretic Phase Changes," *Phys. Fluids* **26** (1983), pp. 2345–2351.

8. M. Johnson and D. Segalman, "A Model for Viscoelastic Fluid Behavior which Allows Non-Affine Deformation," *J. Non-Newtonian Fluid Mech.* **2** (1977), pp. 255–270.

9. R. Kolkka, D. Malkus, M. Hansen, G. Ierley, and R. Worthing, "Spurt Phenomena of the Johnson-Segalman Fluid and Related Models," *J. Non-Newtonian Fluid Mech.* **29** (1988), pp. 303–325.

10. R. Kolkka and G. Ierley, "Spurt Phenomena for the Giesekus Viscoelastic Liquid Model," *J. Non-Newtonian Fluid Mech.*, 1989. To appear.

11. D. Malkus, J. Nohel, and B. Plohr, "Dynamics of Shear Flow of a Non-Newtonian Fluid," *J. Comput. Phys.*, 1989. To appear.

12. T. McLeish and R. Ball, "A Molecular Approach to the Spurt Effect in Polymer Melt Flow," *J. Polymer Sci.* **24** (1986), pp. 1735–1745.

13. J. Nohel, R. Pego, and A. Tzavaras, "Stability of Discontinuous Steady States in Shearing Motions of Non-Newtonian Fluids," *Proc. Roy. Soc. Edinburgh, Series A*, 1989. Submitted.

14. J. Oldroyd, "Non-Newtonian Effects in Steady Motion of Some Idealized Elastico-Viscous Liquids," *Proc. Roy. Soc. London* **A 245** (1958), pp. 278–297.

15. J. Pearson, *Mechanics of Polymer Processing*, Elsevier Applied Science London, 1985.

16. M. Renardy, W. Hrusa, and J. Nohel, *Mathematical Problems in Viscoelasticity*, Pitman Monographs and Surveys in Pure and Applied Mathematics, Vol. 35, Longman Scientific & Technical, Essex, England, 1987.

17. G. Vinogradov, A. Malkin, Yu. Yanovskii, E. Borisenkova, B. Yarlykov, and G. Berezhnaya, "Viscoelastic Properties and Flow of Narrow Distribution Polybutadienes and Polyisoprenes," *J. Polymer Sci., Part A-2* **10** (1972), pp. 1061–1084.

18. M. Yao and D. Malkus, "Analytical Solutions of Plane Poiseuille Flow of a Johnson-Segalman Fluid," in preparation, 1989.